

## Discovery of Selective Inhibitors of Endoplasmic Reticulum Aminopeptidase 1

Zachary Maben,<sup>†,‡</sup> Richa Arya,<sup>†</sup> Digamber Rane,<sup>§</sup> W. Frank An,<sup>||</sup> Shailesh Metkar,<sup>||</sup> Marc Hickey,<sup>||</sup> Samantha Bender,<sup>||</sup> Akbar Ali,<sup>‡,§</sup> Tina T. Nguyen,<sup>‡,#</sup> Irini Evnouchidou,<sup>†,⊥,||</sup> Roger Schilling,<sup>||</sup> Efstratios Stratikos,<sup>⊥</sup> Jennifer Golden,<sup>§,∇</sup> and Lawrence J. Stern<sup>\*,†,‡,§</sup>

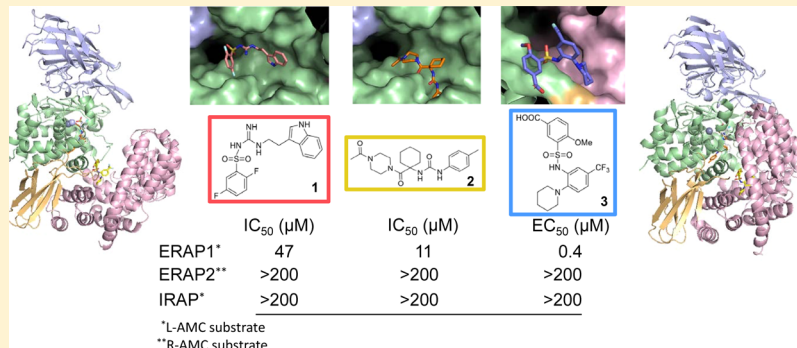
<sup>†</sup>Department of Pathology, and <sup>‡</sup>Department of Biochemistry and Molecular Pharmacology, University of Massachusetts Medical School, Worcester, Massachusetts 01655, United States

<sup>§</sup>Kansas University Specialized Chemistry Center, Lawrence, Kansas 66047, United States

<sup>||</sup>Broad Institute of MIT and Harvard, Cambridge, Massachusetts 02142, United States

<sup>⊥</sup>National Centre for Scientific Research Demokritos, Agia Paraskevi, Athens 15341, Greece

### Supporting Information



**ABSTRACT:** ERAP1 is an endoplasmic reticulum-resident zinc aminopeptidase that plays an important role in the immune system by trimming peptides for loading onto major histocompatibility complex proteins. Here, we report discovery of the first inhibitors selective for ERAP1 over its paralogues ERAP2 and IRAP. Compound 1 (*N*-(*N*-(2-(1*H*-indol-3-yl)ethyl)-carbamimidoyl)-2,5-difluorobenzenesulfonamide) and compound 2 (1-(1-(4-acetylpiperazine-1-carbonyl)cyclohexyl)-3-(*p*-tolyl)urea) are competitive inhibitors of ERAP1 aminopeptidase activity. Compound 3 (4-methoxy-3-(*N*-(2-(piperidin-1-yl)-5-(trifluoromethyl)phenyl)sulfamoyl)benzoic acid) allosterically activates ERAP1's hydrolysis of fluorogenic and chromogenic amino acid substrates but competitively inhibits its activity toward a nonamer peptide representative of physiological substrates. Compounds 2 and 3 inhibit antigen presentation in a cellular assay. Compound 3 displays higher potency for an ERAP1 variant associated with increased risk of autoimmune disease. These inhibitors provide mechanistic insights into the determinants of specificity for ERAP1, ERAP2, and IRAP and offer a new therapeutic approach of specifically inhibiting ERAP1 activity *in vivo*.

### INTRODUCTION

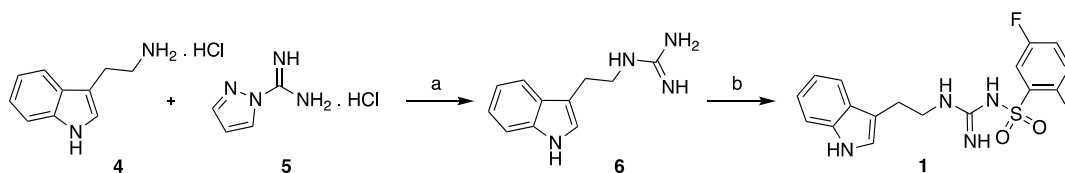
Endoplasmic reticulum aminopeptidase 1 (ERAP1, also known as ARTS1, ALAP, ERAAP, or PILS-AP) is a 107 kDa M1-family zinc aminopeptidase (EC 3.4.11)<sup>1</sup> ubiquitously expressed in somatic cells.<sup>1</sup> ERAP1 trims peptides in the endoplasmic reticulum prior to their presentation on class I major histocompatibility complex (MHC-I) proteins. ERAP1 has length specificity unique among aminopeptidases, efficiently trimming peptides longer than ~8 residues but sparing shorter peptides,<sup>2,3</sup> matching the length preferences of MHC-I.<sup>4</sup> ERAP1 exhibits broad but defined substrate sequence specificity with preference for bulky hydrophobic amino terminal residues and either bulky hydrophobic or basic C-terminal residues.<sup>5,6</sup> ERAP1 is monomeric in solution but exhibits allosteric regulation, with short peptides able to activate ERAP1 for hydrolysis of a model fluorogenic amino

acid substrate leucine-7-amido-4-methylcoumarin (L-AMC).<sup>2</sup> The regulatory site bound by these activator peptides is not known, but has been hypothesized to be distal to the catalytic center, although within the overall binding site for full-length peptide substrates, based on alteration of ERAP1 length dependence in the presence of the allosteric activator, and the ability of some allosteric activators to inhibit full-length peptide hydrolysis. An allosteric model for ERAP1's length dependence has been proposed,<sup>2,7,8</sup> whereby long but not short peptide substrates are able to access the regulatory site, in effect allosterically activating their own hydrolysis.

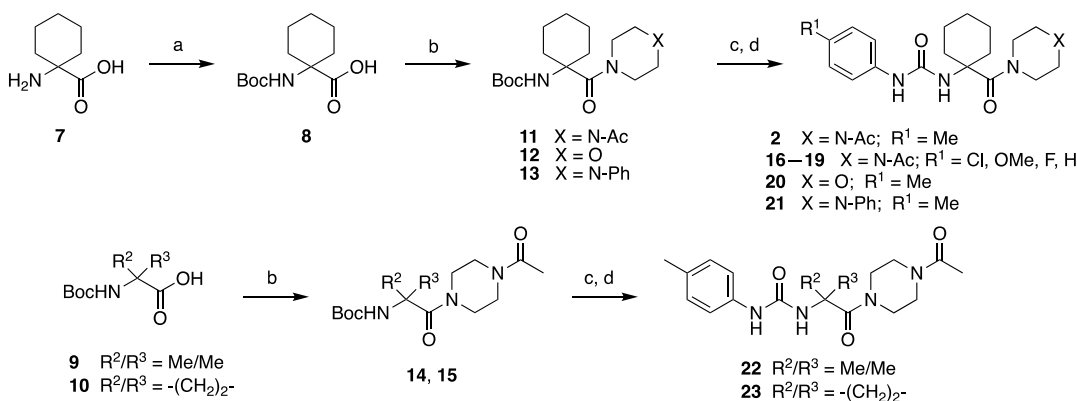
ERAP1 processing can result in generation or degradation of peptides able to bind MHC-I, and as a result, ERAP1 impacts a

Received: February 14, 2019

Published: December 16, 2019

Scheme 1. Synthesis of Compound 1<sup>a</sup>

<sup>a</sup>Reagents and conditions: (a) DIEA, CH<sub>3</sub>CN, RT, 20 h; (b) 2,5-difluorobenzene sulfonyl chloride, NaOH, acetone, RT, 12 h, 35% (over two steps).

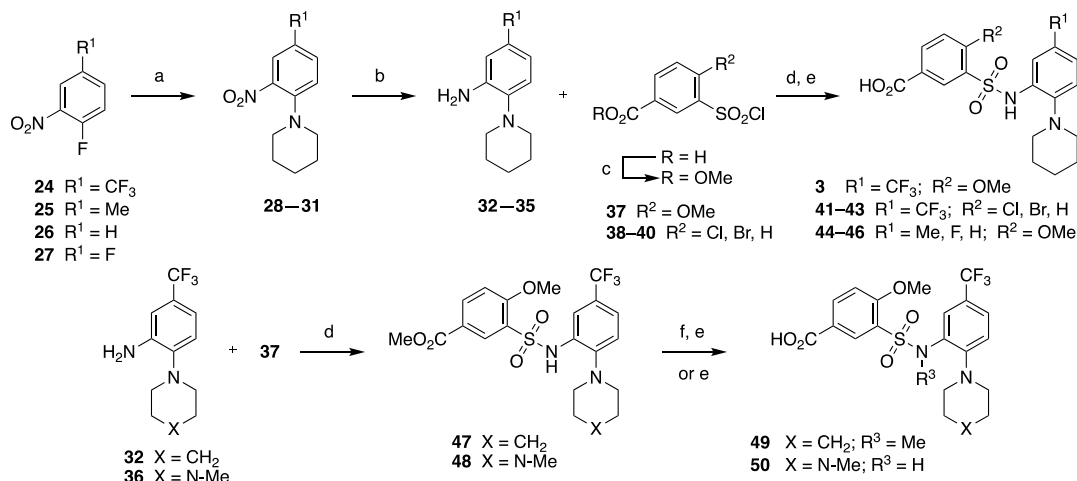
Scheme 2. Synthesis of Compound 2 and Analogues<sup>a</sup>

<sup>a</sup>Reagents and conditions: (a) NaOH, (Boc)<sub>2</sub>O, THF–H<sub>2</sub>O (1:1), RT, 16 h; (b) 4-acetylpiperazine, morpholine, or 4-phenylpiperazine, HATU, DIEA, CH<sub>2</sub>Cl<sub>2</sub>, RT, 16 h, 45–75% (over two steps); (c) TFA, CH<sub>2</sub>Cl<sub>2</sub>, RT, 1 h; (d) DIEA, *p*-tolyl isocyanate or derivative, CH<sub>2</sub>Cl<sub>2</sub>, RT, 8 h, 60–75% (over two steps).

large fraction of the overall MHC-I-bound peptide repertoire.<sup>9–12</sup> After loading, MHC-I molecules traffic to the cell surface where they are assessed by circulating T lymphocytes as part of immune surveillance of bodily tissues for infection or malignancy. Indeed, ERAP1 inhibition has been proposed as a potential approach to enhance the immunogenicity of tumors.<sup>12,13</sup> Polymorphisms in ERAP1, in R528K, are associated with increased susceptibility to T-cell-mediated autoimmune diseases<sup>14</sup> and cancer.<sup>15,16</sup> ERAP1 also has been implicated in regulation of blood pressure<sup>17,18</sup> by hydrolyzing angiotensin II,<sup>19</sup> with secretion of ERAP1 from the ER regulated by thiol reductase ERp44.<sup>17</sup>

In humans, the *erap1* gene is found together with paralogs *ERAP2* and *IRAP* in a gene cluster on chromosome 15, and the corresponding proteins form the oxytocinase subfamily of M1 aminopeptidases. Endoplasmic reticulum aminopeptidase 2 (*ERAP2*, also known as L-RAP, EC 3.4.11) plays a role in antigen processing similar to ERAP1 but with a different substrate peptide sequence preference.<sup>6</sup> Insulin-regulated aminopeptidase (*IRAP*, EC 3.4.11.3), also known as placental leucine aminopeptidase, oxytocinase, and leucyl-cystinyl aminopeptidase, plays an analogous function but in endosomes rather than the endoplasmic reticulum, processing peptides in the MHC-I cross-presentation pathway.<sup>20,21</sup> *IRAP* also performs metabolic, neurological, and endocrine functions.<sup>22–24</sup> Understanding the specific contributions of the different oxytocinase subfamily aminopeptidases is of interest to both basic and applied research. Inhibitors with high selectivity for ERAP1 would allow ERAP1 function to be probed in a manner distinct from genetic deletion,<sup>25</sup> expression modulation via RNAi knockdown,<sup>3</sup> and from less selective inhibitors.<sup>26</sup> However, identification of highly selective inhibitors of ERAP1 has met with limited success despite

many efforts. Commonly used aminopeptidase inhibitors bestatin<sup>27</sup> and amastatin<sup>28</sup> have poor potency for ERAP1<sup>29</sup> and promiscuous inhibition of other aminopeptidases.<sup>30,31</sup> Leucinethiol is somewhat more potent<sup>32</sup> but also inhibits many other peptidases.<sup>33</sup> Many ERAP1 inhibitors act by interaction with the catalytic zinc and surrounding residues, which are well conserved among this enzyme family,<sup>34,35</sup> leading to poor specificity for ERAP1 over other M1 aminopeptidases. One notable example of an ERAP1-specific inhibitor is the compound thiomersal, which is proposed to bind the active site zinc and surrounding residues but could also inactivate the enzyme by nonspecific mechanisms that involve interactions with cysteine residue.<sup>36</sup> Small-molecule inhibitors specific for other M1 aminopeptidases have been identified, including sub-micromolar inhibitors of *IRAP*,<sup>37</sup> human aminopeptidase N/*CD13*,<sup>38</sup> and PfA-M1, an enzyme expressed by *Plasmodium falciparum* during malarial infection.<sup>39,40</sup> Several potent peptide-based inhibitors of M1 aminopeptidases have been developed rationally using a phosphinate group as a substrate transition state analogue.<sup>6,8,41–45</sup> However, as M1 zinc aminopeptidases reaction mechanisms and active site geometry are highly conserved, inhibitors in this class exhibit significant potency for multiple M1 aminopeptidases,<sup>44</sup> although a selective ERAP2 inhibitor in this class was identified<sup>6,8,46</sup> based on ERAP2's unique specificity for basic residues at the P1 site.<sup>4,6</sup> These compounds also may be limited in their *in vivo* utility because of their similarity to peptides, which are hampered by proteolysis and cell membrane impermeability. A fragment-based approach has been applied to the development of small-molecule inhibitors for ERAP1, although selective inhibitors were not identified.<sup>46,47</sup> As ERAP1, ERAP2, and *IRAP* each perform different but related immune functions, the effect of broad inhibition may have dire consequences. The

Scheme 3. Synthesis of Compound 3 and Analogues<sup>a</sup>

<sup>a</sup>Reagents and conditions: (a) piperidine or *N*-methylpiperazine, K<sub>2</sub>CO<sub>3</sub>, DMF, 120 °C, 6 h; (b) SnCl<sub>2</sub>·2H<sub>2</sub>O, EtOH, 70 °C, 1 h, 79% (over two steps); (c) SOCl<sub>2</sub>, RT, 16 h, then MeOH, RT, 2 h, quant.; (d) pyridine, RT, 16 h; (e) LiOH·H<sub>2</sub>O, THF–H<sub>2</sub>O (1:1), RT, 8 h, 25–35% (over two steps); (f) NaH, MeI, DMF, RT, 18 h, 25%.

clinical implications of either specific or broad inhibition of oxytocinase M1 aminopeptidases are still unknown but may have a significant impact on treating human diseases.<sup>48,49</sup>

In this study, we developed a high-throughput screening (HTS) strategy to identify small-molecule inhibitors selective for ERAP1 over the other oxytocinase family aminopeptidases ERAP2 and IRAP. Compounds with three different chemical frameworks were identified for optimization and tested using physiologically relevant substrate processing assays. Compounds 2 and 3 also inhibit ERAP1's activity in cellular antigen processing assay. Molecular docking, mechanism of action studies, and mutagenesis results indicate that compounds 1 and 2 target ERAP1's active site, whereas compound 3 targets an allosteric regulatory site.

## CHEMISTRY

Compound 1 was synthesized from tryptamine hydrochloride in two steps as outlined in Scheme 1. Briefly, reaction of tryptamine hydrochloride 4 with 1*H*-pyrazole-1-carboximidate hydrochloride 5 in the presence of *N,N*-diisopropylethylamine (DIEA) in CH<sub>3</sub>CN provided the corresponding guanidinium intermediate 6. The crude product 6 was reacted with 2,5-difluorobenzene sulfonyl chloride in the presence of NaOH in acetone to afford 1 in 35% yield over two steps.

Compound 2 and analogues were prepared from commercially available amino acids in four steps involving protection of amino groups, amide coupling, deprotection, and urea formation. As shown in Scheme 2, the unnatural amino acid homocycloleucine 7 was treated with di-*tert*-butyl dicarbonate and NaOH in tetrahydrofuran (THF)–H<sub>2</sub>O mixture to afford the corresponding Boc-protected derivative 8. The Boc-protected amino acid derivatives 9–10 were prepared using the same conditions. The carboxylic acids 8–10 were coupled with *N*-acetylpiperazine, morpholine, or *N*-phenylpiperazine using 1-[bis(dimethylamino)-methylene]-1*H*-1,2,3-triazolo-[4,5-*b*]pyridinium 3-oxid hexafluorophosphate (HATU) and DIEA to provide amides 11–15. Removal of the Boc protecting group with TFA and reaction of the resulting amine salts with *p*-tolyl isocyanate or derivative provided the target urea compound 2 and analogues 16–23 (Scheme 2).

Arylsulfonamide 3 and analogues were prepared from the corresponding phenyl-piperidine and phenyl-piperazine derivatives as outlined in Scheme 3. The required intermediates were prepared in two steps involving an S<sub>N</sub>Ar reaction of 5-substituted 2-fluoronitrobenzene 24–27 with the cyclic amines followed by the reduction of the nitro group with SnCl<sub>2</sub>·2H<sub>2</sub>O to afford anilines 32–36. The sulfonyl chlorides 37–40 were either commercially available or prepared from the corresponding 4-substituted (3-chlorosulfonyl)benzoic acid derivatives by esterification using thionyl chloride and MeOH. Finally, reactions of substituted anilines 32–35 with 2,5-substituted benzenesulfonyl chlorides 37–40 in pyridine followed by ester hydrolysis using LiOH·H<sub>2</sub>O afforded the target compound 3 and analogues 41–46. Treatment of sulfonamide 47 with NaH and MeI in dimethylformamide (DMF) followed by ester hydrolysis provided the *N*-methyl derivative 49. The 4-methylpiperazine analogue 50 was synthesized from the aniline derivative 36 using the above general reaction sequence (Scheme 3).

## RESULTS

**MLPCN Library Screen.** ERAP1 enzymatic activity can be conveniently assayed using the synthetic fluorogenic substrate L-AMC.<sup>50</sup> Because this is shorter than preferred substrates, ERAP1 hydrolysis activity of L-AMC is substantially lower than for more physiologically relevant peptides of eight or more residues<sup>2</sup> but can be measured easily by fluorescence in microtiter format HTS assays. In order to identify novel ERAP1-selective inhibitors, we designed and implemented a HTS of the NIH's Molecular Libraries Probe Production Centers Network (MLPCN) >350 000 compound library at the Broad Institute's Probe Development Center. We screened for compounds that inhibit ERAP1 L-AMC hydrolysis activity at a single concentration point (10.7 μM) (Figure 1). Compounds that decreased ERAP1 L-AMC hydrolysis activity by 30% were filtered to remove promiscuous hit compounds (compounds with greater than 5% hit rate in PubChem assay records). Additionally, known metal chelators, electrophiles, and compounds qualifying as PAINS were omitted from the candidate pool. Compounds containing peptidomimetic motifs

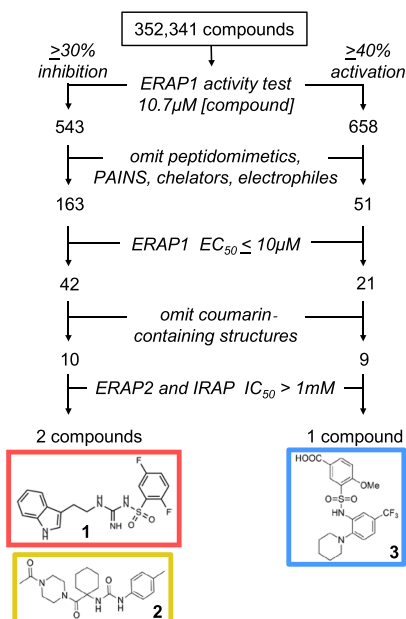


**Figure 1.** Screening pathway. The MLPCN library was screened for alteration of ERAP1 activity. Inhibitors and activators were examined to remove known problematic scaffolds and moieties (PAINS) as well as peptidomimetic compounds. Remaining compounds were then tested for potency with a cutoff half-maximal effective concentration ( $EC_{50}$ ) of  $10 \mu\text{M}$ . We observed several candidate compounds containing coumarinyl groups and removed them out of concern for false positives. We then counter-screened the compound pools for activity on ERAP2 and IRAP. Two L-AMC hydrolysis inhibitors (1 and 2) and one L-AMC hydrolysis activator (3) were identified.

were omitted in order to define a pool of hit compounds with modes of inhibition distinct from previously characterized inhibitors of M1 family aminopeptidases. Compounds containing coumarinyl moieties were also omitted to minimize false positive results from autofluorescent compounds, as our initial activity assay monitored fluorescence of 7-amino-4-methylcoumarin (AMC) as a reporter of aminopeptidase-catalyzed L-AMC hydrolysis. Remaining hit compounds were subsequently tested for dose-dependent efficacy against ERAP1, and candidates with half-maximal inhibitory concentration ( $IC_{50}$ ) for L-AMC hydrolysis weaker than  $10 \mu\text{M}$  were removed from consideration. Potency was quantified by fitting data with sigmoidal functions anchored to an uninhibited control as curve maximum and a curve minimum greater than zero activity. Compounds exhibiting dose-dependent inhibition were then counter-screened for hydrolysis inhibition of IRAP (L-AMC substrate) or ERAP2 (arginine-7-amido-4-methylcoumarin (R-AMC) substrate), removing hits with  $IC_{50}$  lower than  $1 \text{ mM}$  for either ERAP2 or IRAP. We identified two compounds as selective inhibitors of ERAP1-catalyzed hydrolysis of L-AMC, designated here as 1 and 2.

Based on previous work demonstrating allosteric activation of ERAP1,<sup>2,7</sup> we also screened for compounds in the MLPCN library that increased ERAP1-catalyzed L-AMC hydrolysis. Previous studies have shown that certain short peptides and nonhydrolyzable substrates can activate ERAP1 L-AMC hydrolysis but inhibit processing of full-length peptides, which are more physiologically relevant ERAP1 substrates.<sup>2</sup> The mechanism proposed for such behavior was binding to an allosteric regulatory site that promoted a domain closure required for active-site reorganization and L-AMC hydrolysis;

in the hypothesized mechanism, this site overlapped with the binding site for full-length peptide substrates.<sup>2</sup> Thus, occupancy of the regulatory site would competitively inhibit processing of full-length peptide substrates (see Supporting Information, Figure S1). We hypothesized that compounds that activate ERAP1-catalyzed L-AMC hydrolysis might similarly act as inhibitors for full-length peptide processing by occupying a regulatory site within the overall substrate binding envelope. We initially selected compounds that increased L-AMC hydrolysis by 40% [3 standard deviations (SDs)] over untreated control for further characterization (Figure 1, right side). Candidate activator compound screens proceeded as with inhibitors, with manual identification of metal chelators, electrophiles, PAINS compounds, peptidomimetics, and promiscuous positive hit compounds (using the same 5% positive PubChem hit rate cutoff as before). Activator dose-dependent potency was then assayed for half-maximal activating concentration ( $AC_{50}$ ) better than  $10 \mu\text{M}$ . As compounds exhibited different levels of maximum activation, dose-dependent hydrolysis data were fit using sigmoidal functions anchored to an uninhibited control with no restraint on curve maximum. Compounds with sufficient activating potency were then counter-screened for ERAP2 or IRAP activity (either activation or inhibition) as before. We identified one ERAP1-selective activator, compound 3. Compounds 1, 2, and 3 and analogues were synthesized for confirmatory testing, structure–activity relationship (SAR) analysis, mechanism of action, and functional testing.

#### Dose Dependence and Specificity of Hit Compounds.

We tested the synthesized compounds 1, 2, and 3 in dose-dependent L-AMC hydrolysis assay (Figure 2A). Compounds

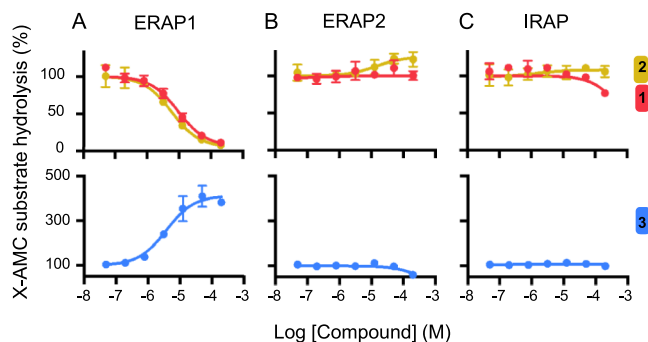


**Figure 2.** Compounds 1, 2, and 3 are highly specific for ERAP1. Enzyme activity was measured using dipeptide substrate analogue X-7-amido-4-methylcoumarin (X-AMC), where the amino-terminal residue X is leucine (ERAP1, IRAP) or arginine (ERAP2), corresponding to the substrate preference of each enzyme.<sup>21</sup> Hydrolysis was measured over a range of compound concentrations for (A) ERAP1, (B) ERAP2, or (C) IRAP. Activity was normalized to the activity of the enzyme in the presence of DMSO. Representative data (mean  $\pm$  SD,  $n = 3$ ) from one of two experiments are shown. Data points were fit using a sigmoidal curve with the top or bottom value for inhibitor or activator curves, respectively, constrained to 100%.  $EC_{50}$  values shown in Supporting Information, Table S1.

1 and 2 exhibited ERAP1 L-AMC  $IC_{50}$  of  $9.2$  and  $6.9 \mu\text{M}$ , respectively. We confirmed the specificity of these compounds observed in the MLPCN screen for ERAP1 over homologues ERAP2 and IRAP. All three compounds are more than 100-fold more selective for ERAP1 than for ERAP2 (Figure 2B) or IRAP (Figure 2C), and in some cases, no activity at all on ERAP2 and IRAP was detected. Compound 3 activated

ERAP1 hydrolysis of L-AMC (Figure 2A, lower panel), with an  $AC_{50}$  of 4.1  $\mu\text{M}$  and a maximum activity enhancement of 4.1-fold over control. This compound is a very weak inhibitor of ERAP2 with an  $IC_{50}$  greater than 200  $\mu\text{M}$  and has no detectable effect on IRAP activity (Figure 2B,C, lower panels).

We tested the effect of these inhibitors on ERAP1-catalyzed hydrolysis of a decamer peptide WRCYKEMALK (WK10),<sup>51</sup> which represents a more physiologically relevant ERAP1 substrate than L-AMC. ERAP1 efficiently hydrolyzed the N-terminal tryptophan and released the nonamer product peptide RCYKEMALK (Figure 3A). Removal of the subsequent amino

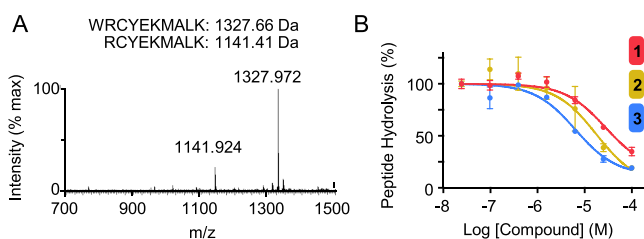


**Figure 3.** Compounds 1, 2, and 3 inhibit ERAP1-catalyzed peptide hydrolysis. (A) ERAP1 hydrolysis of the N-terminal tryptophan from the peptide WRCYKEMALK (WK10). MALDI spectrum after 30 min incubation with ERAP1. Calculated masses are shown at top, and the observed peak  $m/z$  is displayed on the graph. (B) Compound dose–response of ERAP1-catalyzed peptide hydrolysis inhibition. Representative data ( $n = 2$ ) normalized to DMSO control condition shows inhibition of peptide hydrolysis.  $IC_{50}$  values shown in Supporting Information, Table S1.

acid arginine was inefficient, consistent with ERAP1's amino-terminal substrate specificity.<sup>1</sup> Here, we quantified product peptide production by liquid chromatography–mass spectrometry (LC–MS) rather than fluorescence, which does not require introduction of the non-natural fluorescence-quenching dinitrophenyl maleimide as in the original assay.<sup>51,52</sup> Both compounds 1 and 2 inhibited peptide hydrolysis in a dose-dependent manner (Figure 3B). Compound 3, identified as an activator of ERAP1 L-AMC hydrolysis, also inhibited peptide hydrolysis in a dose-dependent manner (Figure 3B), as previously observed for short peptides that activate L-AMC hydrolysis.<sup>2</sup> The  $IC_{50}$  values for WK10 peptide hydrolysis showed the same rank order and relative potency as the

respective  $IC_{50}$  values for L-AMC hydrolysis (Supporting Information, Table S1).

**SAR Studies.** Of the compounds identified as inhibitors or activators of ERAP1 hydrolysis of L-AMC, compound 2 and 3 were selected for SAR analysis. For compound 2, modification of the *N*-acetylpiperazine and homocycloleucine moieties generally resulted in loss of potency of one log or more; however, substitutions on the aromatic ring were better tolerated (Table 1, Supporting Information, Figure S2). Compound 16, wherein the *p*-tolyl group is replaced with a 4-chlorophenyl group, showed a small improvement in potency in both L-AMC and WK-10 peptide hydrolysis assays. The *N*-acetyl group on piperazine was critical for the activity, as analogues with morpholine (compound 20) and *N*-phenylpiperazine (compound 21) had no detectable inhibitory activity (Table 1).

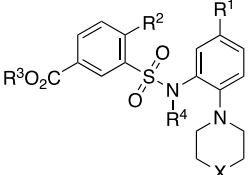
SAR exploration of compound 3 provided several analogues with similar or slightly improved potency (Table 2, Supporting Information, Figure S3). Substitutions of the trifluoromethyl ( $R^1$ ) and methoxy ( $R^2$ ) groups on the two aromatic rings were largely tolerated but resulted in lower potency. Compound 41, where the methoxy group was replaced with a chloro group showed a 5-fold loss in potency, whereas compound 42 with a bromo substitution was only 2-fold less active than 3. Replacement of the trifluoromethyl group with a methyl (compound 44) or fluoro group (compound 45) resulted in about 8-fold loss in potency, though the unsubstituted analogue (compound 46) maintained better potency. The aromatic carboxylic acid appeared to be essential for activation of ERAP1's L-AMC hydrolysis activity, as the methyl ester 47 had no detectable activity in this assay, although surprisingly WK10 peptide hydrolysis inhibition was largely intact. This was the only compound for which such discordant activity was observed. Methylation of the sulfonamide nitrogen gave analogue 49, which was also about 10-fold less active. Compound 50, with the *N*-methylpiperazine moiety instead of piperidine, had equivalent activity to the parent compound 3 (Table 2, Supporting Information, Figure S3).

**Mechanism of Action Studies.** To help understand the mechanism of action of these compounds, we evaluated ERAP1 enzyme activity at various concentrations of substrate and inhibitors. We used the chromogenic substrate leucine *p*-nitroanilide (L-pNA) instead of fluorogenic L-AMC, so that a wider range of substrate concentrations could be investigated.

**Table 1.**  $IC_{50}$  Values of Compound 2 and Analogues

compound	X	$R^1$	$R^2/R^3$	ERAP1 L-AMC $IC_{50}$ ( $\mu\text{M}$ )	ERAP2 R-AMC $IC_{50}$ ( $\mu\text{M}$ )	IRAP1 L-AMC $IC_{50}$ ( $\mu\text{M}$ )	ERAP1 WK10 peptide $IC_{50}$ ( $\mu\text{M}$ )
2	N-Ac	Me	$-(\text{CH}_2)_5-$	6.9	>200	>200	6.9 <sup>a</sup>
16	N-Ac	Cl	$-(\text{CH}_2)_5-$	3.6	>200	>200	4.3
17	N-Ac	OMe	$-(\text{CH}_2)_5-$	115 <sup>a</sup>	>200	>200	31.8
18	N-Ac	F	$-(\text{CH}_2)_5-$	>200	>200	>200	~165 <sup>a</sup>
19	N-Ac	H	$-(\text{CH}_2)_5-$	20.6 <sup>a</sup>	>200	>200	~135 <sup>a</sup>
20	O	Me	$-(\text{CH}_2)_5-$	>200	>200	>200	>200
21	N-Ph	Me	$-(\text{CH}_2)_5-$	>200	>200	>200	~124
22	N-Ac	Me	Me/Me	126	>200	>200	150
23	N-Ac	Me	$-(\text{CH}_2)_2-$	>200	>200	>200	170 <sup>a</sup>

<sup>a</sup>Partial inhibition, with less than 90% inhibition observed at the highest concentration tested (see Supporting Information, Figure S2).

Table 2. IC<sub>50</sub> Values of Compound 3 and Analogues


compound	X	R <sup>1</sup>	R <sup>2</sup>	R <sup>3</sup> , R <sup>4</sup>	ERAP1 L-AMC		ERAP2 R-AMC		IRAP1 L-AMC	ERAP1 WK10 peptide
					IC <sub>50</sub> (μM)	AC <sub>50</sub> (μM) (fold) <sup>a</sup>	IC <sub>50</sub> (μM)	AC <sub>50</sub> (μM) (fold) <sup>a</sup>	IC <sub>50</sub> (μM)	IC <sub>50</sub> (μM)
3	CH <sub>2</sub>	CF <sub>3</sub>	OMe	H, H		4.1 (4.1)	>200		>200	5.3
41	CH <sub>2</sub>	CF <sub>3</sub>	Cl	H, H		21.2 (3.7)	>200		>200	15.2
42	CH <sub>2</sub>	CF <sub>3</sub>	Br	H, H		10.9 (3.3)	>200		>200	8.2
43	CH <sub>2</sub>	CF <sub>3</sub>	H	H, H		35.9 (3.5)	~140		>200	20.2
44	CH <sub>2</sub>	Me	OMe	H, H		32.9 (1.5)	ND <sup>b</sup>		>200	7.4
45	CH <sub>2</sub>	F	OMe	H, H		29.1 (1.4)	159		>200	8.6
46	CH <sub>2</sub>	H	OMe	H, H		11.6 (1.4)	81.2		>200	14.4
47	CH <sub>2</sub>	CF <sub>3</sub>	OMe	Me, H	>200			~42 (1.2)	>200	6.9
49	CH <sub>2</sub>	CF <sub>3</sub>	OMe	H, Me		50.3 (2.7)	~160		~160	32.6
50	N-Me	CF <sub>3</sub>	OMe	H, H		2.9 (3.1)	ND		>200	3.0

<sup>a</sup>Fold increase in hydrolysis activity. <sup>b</sup>ND: not determined.

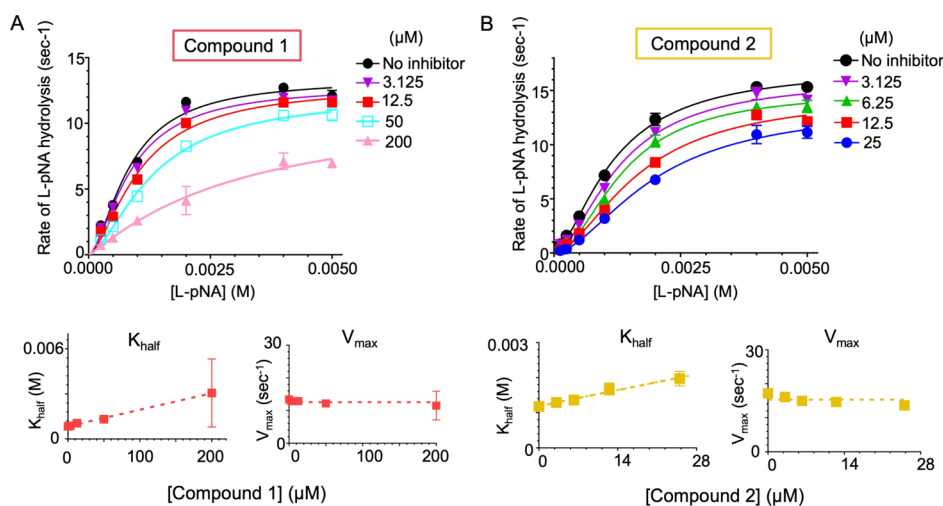


**Figure 4.** Mechanism of action studies for (A) compound 1 and (B) compound 2. Top, initial rates of L-pNA hydrolysis by ERAP1 in the presence of various concentrations of the inhibitor. Initial rate versus substrate concentration curves obtained at various inhibitor concentrations were fit to an allosteric Michaelis–Menten equation to obtain values for  $V_{max}$  and for  $K_{half}$ , an allosteric equivalent to  $K_m$  (see the [Experimental Section](#) for details). Bottom, the resulting values for  $K_{half}$  and  $V_{max}$  with uncertainly estimates are plotted as a function of inhibitor concentration to help determine the inhibitor mechanism of action.

We measured initial rates under steady-state conditions and analyzed the data using a Michaelis–Menten framework with a cooperativity term (Hill coefficient) to account for the allosteric behavior of ERAP1 toward short substrates (see the [Experimental Section](#)).<sup>2</sup> L-pNA hydrolysis in the absence of the inhibitor had the following parameters:  $h = 1.45 \pm 0.15$ ,  $K_{half} = 1.41 \pm 0.16$  mM, and  $V_{max} = 17.25 \pm 1.05$  s<sup>-1</sup>, where  $h$  is the Hill coefficient,  $K_{half}$  is the concentration of the substrate at which the half-maximal rate is observed and is the allosteric equivalent of the conventional Michaelis constant  $K_m$ , and  $V_{max}$  is the maximum reaction rate ([Supporting Information](#), Table S2). For compound 1, increasing inhibitor concentrations resulted in decreased L-pNA hydrolysis activity ([Figure 4A](#)). The apparent Michaelis constant  $K_{half}$  increased linearly with increasing inhibitor concentration, without apparent change in  $V_{max}$ , consistent with a competitive inhibition mechanism. The full set of curves were described well by an equation describing

competitive inhibition in an allosteric setting (see the [Experimental Section](#), competitive allosteric inhibition)  $K_i = 51.7 \pm 4.3$  μM ([Supporting Information](#), Table S1). For compound 2 ([Figure 4B](#)), similar behavior was observed, with fit values for  $K_{half}$  increasing linearly with inhibitor concentration, fit values for  $V_{max}$  not significantly changing. As with compound 1, this behavior is consistent with a competitive mode of inhibition. Best fit value for  $K_i$  was  $12.8 \pm 1.0$  μM ([Supporting Information](#), Table S1).

For compound 3, increasing concentrations resulted in increased rather than decreased L-pNA hydrolysis activity, across a range of substrate concentrations ([Figure 5A](#)). This behavior indicates that compound 3 is acting as a nonessential activator of L-pNA hydrolysis, with activity ( $V_{max}/K_{half}$ ) increasing up to 1.8-fold over the concentration range tested. However, different behavior was observed for compound 3 when a full-length peptide (LF9, LVAFKARKF)<sup>5</sup> was used as a

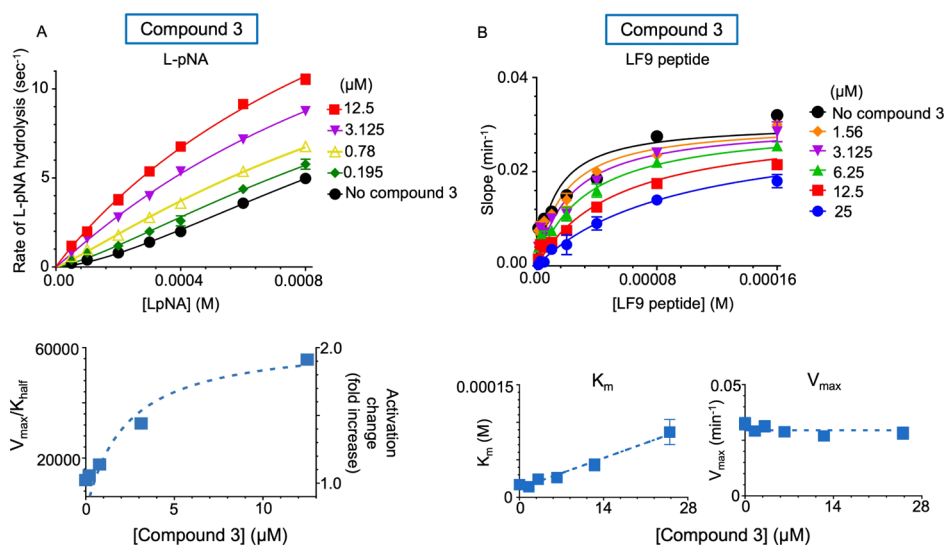


**Figure 5.** Mechanism of action studies for compound 3. Initial rates of (A) L-pNA or (B) LF9 peptide hydrolysis by ERAP1 in the presence of various concentrations of compound 3. Top, initial rate versus substrate concentration curves obtained at various inhibitor concentrations were fit to an allosteric Michaelis–Menten equation for L-pNA hydrolysis or a conventional Michaelis–Menten equation for LF9 peptide hydrolysis. Bottom, the resultant values for  $V_{\max}/K_{\text{half}}$  (for L-pNA) or for  $K_m$  and  $V_{\max}$  (for LF9 peptide) with uncertainty estimates are plotted as a function of compound 3 concentration to help determine the mechanism of action.

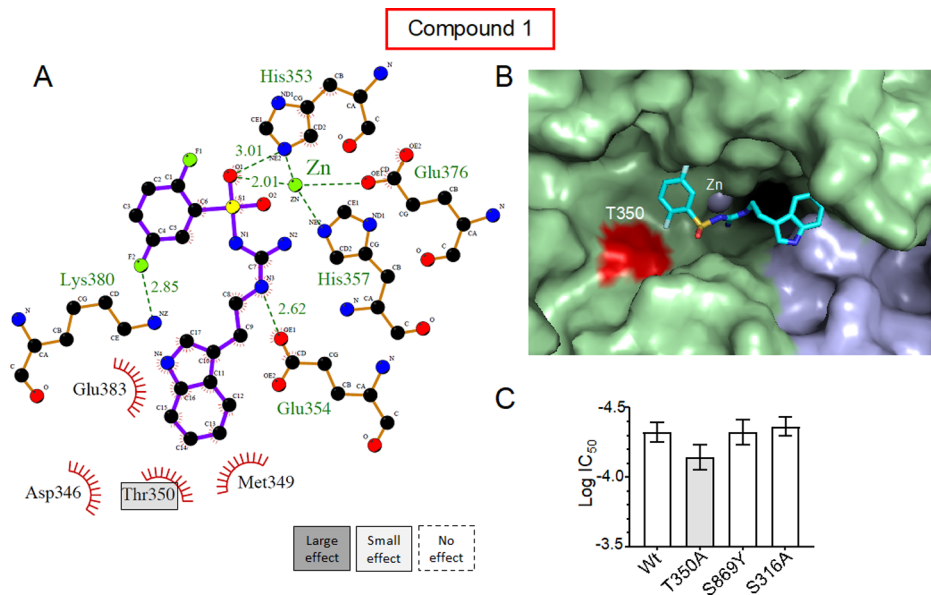


**Figure 6.** In silico docking sites and experimental validation for compound 1. (A) Environment around the preferred docking pose as shown by LigPlot+.<sup>57</sup> Alternate docking pose (in PDB 2YD0) is shown in Supporting Information, Figure S4. Boxes indicate positions of residues mutated to corresponding ERAP2 or IRAP residues in order to validate the docking pose. (B) Docking pose of compound 1 in the surface structure of open ERAP1, with domain I shown in light blue, domain II in green, and mutation position in red. (C) L-AMC  $IC_{50}$  values for mutant proteins (Supporting Information, Table S3). PDB 6MGQ was used for docking.

substrate instead of L-pNA (Figure 5B). Here, we used coupled enzyme assay to follow removal of the N-terminal leucine (see the Experimental Section). ERAP1 hydrolysis of full-length peptides is not cooperative,<sup>2,53</sup> and initial rate curves in the absence of inhibitor were fit with  $K_m = 0.024 \pm 0.006$  mM.  $K_m$  values increased linearly with increasing inhibitor concentration, while  $V_{\max}$  remained essentially unchanged (Figure 5B). These data were described best by an equation defining conventional competitive inhibition (see the Experimental Section, competitive inhibition) with  $K_i = 3.8 \pm 0.7$   $\mu\text{M}$  (Supporting Information, Table S1).

**Molecular Docking and Validation.** To help rationalize the different behaviors observed for compounds 1, 2, and 3, and to identify possible binding sites, we used an in silico docking approach. Compound docking was performed using the Glide module from the Schrödinger software package, and binding site solutions were further analyzed by running Embrace minimization on the docked structure. ERAP1 has been proposed to cycle between open and closed conformations during the catalytic cycle,<sup>2,53,54</sup> and so we used as targets for the in silico docking procedure coordinates from crystal structures of ERAP1 in both open (PDB 6MGQ) and closed (PDB 2YD0) conformations.

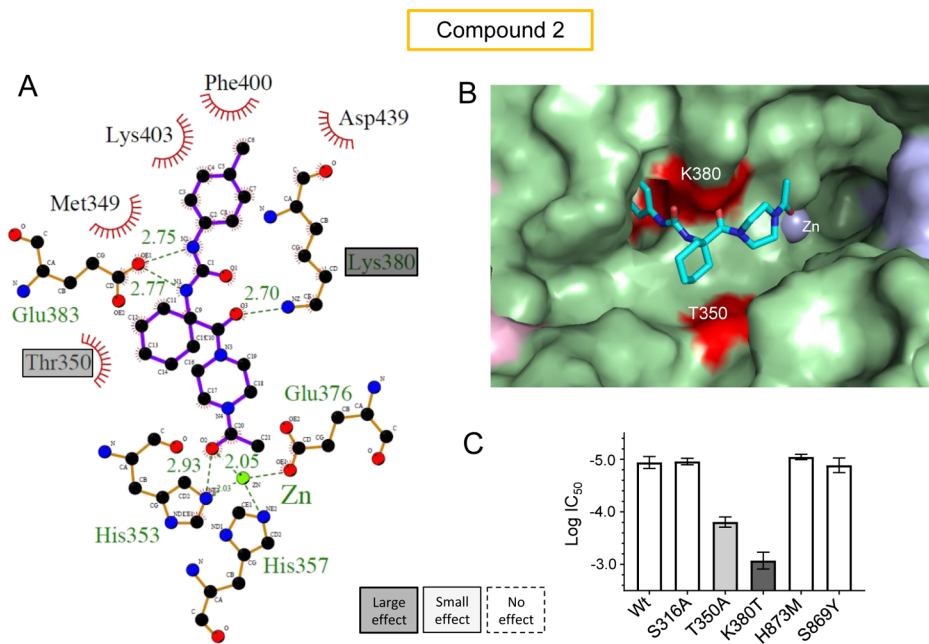


**Figure 7.** In silico docking sites and experimental validation for compound 2. (A) Environment around the preferred docking site shown as LigPlot+.<sup>57</sup> Alternate docking pose is (in PDB 2YD0) shown in Supporting Information, Figure S7. Boxes indicate positions of residues mutated to corresponding ERAP2 or IRAP residues to validate the docking pose. (B) Docking pose of compound 2 in the surface structure of open ERAP1, with domain I shown in light blue, domain II in green, domain IV in pink, and mutation positions in red. (C) L-AMC  $IC_{50}$  values for mutant proteins (Supporting Information, Table S3). PDB 6MGQ was used for docking.

For compound 1, the top docking solution for either open or closed conformations was at the active site, partially overlapping with substrates modeled into these structures based on bound inhibitors (bestatin for 2YD0, phosphinic peptide for 6MGQ). In the top predicted binding pose for the open conformation docking solution (Figure 6A,B), the inhibitor's sulfonamide group engaged the catalytic zinc, similar to the binding mode observed or predicted for other sulfonamide-based M1-family peptidase inhibitors.<sup>55,56</sup> In the top closed conformation docking solution, the sulfonamide was displaced from the zinc center by approximately 4 Å, and the positions of the indole and difluorobenzene moieties were flipped (Supporting Information, Figure S4). To help distinguish these possibilities, we compared the active sites of ERAP1 with ERAP2 (PDB 6EA4, closed conformation) and IRAP (PDB 4Z71 and PDB 5MJ6, partially open and closed conformations, respectively) because these proteins were >1000-fold less sensitive to inhibition by compound 1. We identified residues in contact with compound 1 for each of the predicted binding poses and replaced these either with homologous ERAP2 or IRAP residues or with alanine. Thus, we prepared ERAP1 proteins with a substitution at position T350, predicted to contact compound 1 indole ring if the open-conformation docking mode was correct, at position S869, predicted to contact the indole ring if the closed-conformation docking mode were correct, or at position S316, predicted to interact with one of the fluoro groups on the phenyl ring in the closed but not open-docking mode. ERAP1 mutants T350A, S869Y, and S316A retained L-pNA hydrolysis activity, although S869Y activity was reduced fivefold (Supporting Information Figure S5, Table S2). We measured sensitivity of these mutant ERAP1 proteins for compound 1, using L-AMC inhibition assay (Figure 6C, Supporting Information Figure S6, Table S3). A small reduction in potency was observed for T350A. This is consistent with the docking mode identified for the open

conformer shown in Figure 6A, as well as the observed competitive mode of action, but given the uncertainties in docking and the lack of robust effects observed with mutagenesis, the predicted binding site should be considered provisional.

For compound 2, the top docking solutions to open and closed ERAP1 conformers again were found at the active site, overlapping with the expected substrate binding site. Two very similar potential binding poses were identified, with the terminal *N*-acetylpiperazine carbonyl group coordinating the catalytic zinc in the open conformer docking solution (Figure 7A,B) and the central urea oxygen coordinating zinc in the closed conformer solution (Supporting Information, Figure S7). Again, we identified residues from ERAP1 that contacted the inhibitor bound in either of the two predicted binding poses and prepared mutant proteins with residues from either ERAP2 or IRAP that would be predicted to impact inhibitor binding: K380T predicted to disrupt contacts with compound 2 in the open conformer binding solution, and S316A, H873M, and S869Y predicted to disrupt contacts in the closed conformer binding solution. We also mutated residue T350 to alanine; in ERAP1, this residue contacts the compound 2 cyclohexyl group in either of the two predicted binding poses. All of the mutants retained activity, although  $K_m$  and/or  $V_{max}$  values were altered 10-fold for K380T (Supporting Information Figure S5, Table S2). L-AMC inhibition studies with the mutant proteins revealed a large effect of K380T, with 80-fold increase in the  $IC_{50}$  value and a smaller but still substantial 10-fold increase in  $IC_{50}$  for T350A (Figure 7C, Supporting Information Figure S6, Table S3). None of the other mutants appreciably affected compound 2 potency. These results are consistent with the docking pose identified using the open conformer of ERAP1 (Figure 7A) but not the pose identified using the closed conformer (Supporting Information, Figure S7). The preferred docking pose has the ERAP1 zinc atom



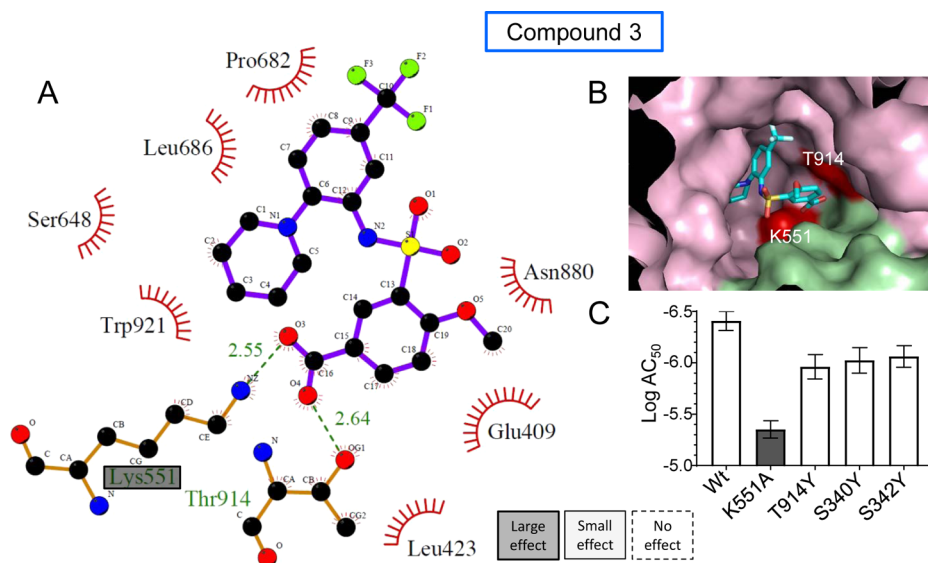


**Figure 8.** In silico docking sites and experimental validation for compound 3. (A) Environment around the preferred docking site shown as LigPlot+. Alternate docking pose is shown in Supporting Information, Figure S8. Boxes indicate positions of residues mutated to corresponding ERAP2 or IRAP residues to validate the docking pose. (B) Docking pose of compound 3 in the surface structure of closed ERAP1, with domain II shown in green, domain IV in pink, and mutation positions in red. (C) L-AMC AC<sub>50</sub> values for mutant proteins (Supporting Information, Table S3). PDB 2YD0 was used for docking.

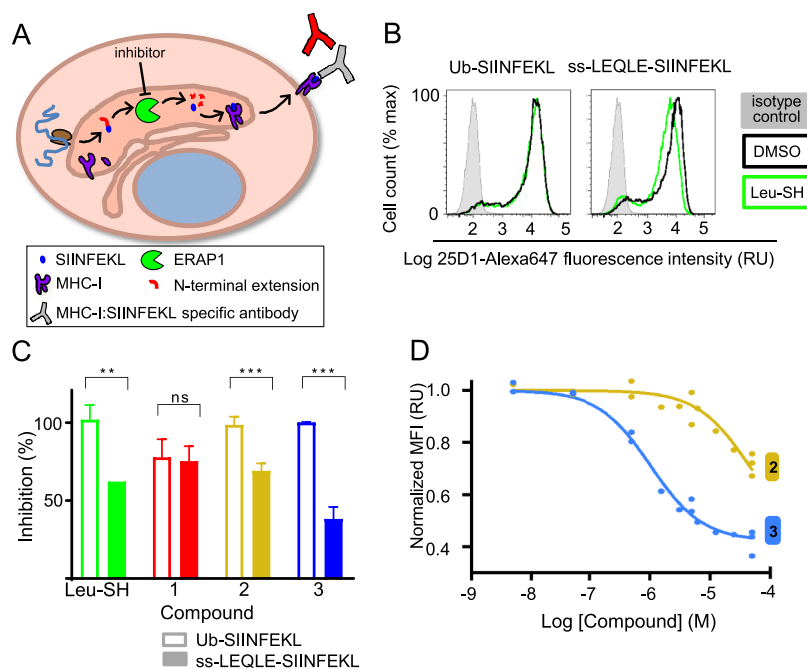


**Figure 9.** Compounds 2 and 3 inhibit ERAP1 activity in cellular context. (A) Schematic depiction of the experiment. HeLa cells expressing the MHC-I protein K<sup>b</sup> were infected with recombinant vaccinia virus construct that directs expression and ER-transport of the SIINFEKL peptide with N-terminal extension LEQLE. ERAP1 must trim the peptide to allow binding to the MHC-I protein. ERAP1 activity is quantified by measuring the surface MHC-I:SIINFEKL complex with a specific antibody. (B) ERAP1 processing of the N-extended ERAP1-dependent substrate ss-LEQLE-SIINFEKL or control ERAP1-independent substrate Ub-SIINFEKL, evaluated by comparing MHC-I:SIINFEKL production in cells treated with the nonspecific zinc peptidase inhibitor leucinethiol (Leu-SH, 50  $\mu$ M) or vehicle only [dimethyl sulfoxide (DMSO)]. Samples are gated on GFP+ singlets (see Supporting Information, Figure S9) prior to quantitation of 25D1 mean fluorescence intensity (MFI) indicative of the level of surface K<sup>b</sup>:SIINFEKL complex. (C) Compounds 2 and 3 but not compound 1 specifically inhibit ERAP1-dependent cellular processing activity. Percent inhibition calculated for cells treated with 50  $\mu$ M compound relative to cells treated with vehicle only. Results from triplicate samples from two independent assays are shown. Significance evaluated by unpaired two-way Student's *t*-test: \*\**p* < 0.005; \*\*\**p* < 0.001. (D) Compounds 2 and 3 are active in cell processing assay in a dose-dependent manner. Normalized MFI values are ratios of ss-LEQLE-SIINFEKL to Ub-SIINFEKL staining. Data points from three separate titration experiments are plotted together with one global sigmoidal curve calculated for each compound.

coordinated by an *N*-acetyl carbonyl group,<sup>58</sup> substitution of which in compounds 20 and 21 substantially reduced potency,

and it is possible that replacement of the *N*-acetylpiperazine with 4-carboxypiperidine or the corresponding carbamate

would increase potency, similar to a strategy used to optimize aminopeptidase N inhibitors.<sup>59</sup>

For compound 3, the top in silico docking solutions outside the active site were found at the junction of domains II and IV. (We did not consider docking solutions with any atom within 6 Å of the catalytic zinc, because compound 3 acts to activate L-AMC and L-pNA hydrolysis, implying that it binds at a site distinct from these substrates). One potential binding site (Figure 8A,B) was found similarly using both open and closed ERAP1 conformers as docking targets; another potential binding site with similar docking energy (Supporting Information Figure S8) was found only using the closed conformer. For each of the predicted binding sites, we identified ERAP1 residues interacting with compound 3 that would be disrupted by substitution of homologous residues from ERAP2 or IRAP. By this analysis, ERAP1 mutations K551A and T914Y are predicted to disrupt electrostatic and hydrogen-bonding interactions with compound 3 bound in the shared predicted docking site, and S340Y and S342Y are predicted to disrupt similar contacts with compound 3 bound in the docking site predicted only in the closed conformation. Recombinant proteins carrying these mutations individually had enzymatic parameters similar to those of wild-type ERAP1 (Supporting Information, Figure S5; Supporting Information, Table S2). A substantial effect was observed only for the K551A mutation (Figure 8C, Supporting Information, Figure S6, and Table S3), favoring the shared site as shown in Figure 8A.

**Cellular Inhibition Studies.** Among potential uses of specific ERAP1 inhibitors is the application of these compounds in vivo for therapeutic treatment. To evaluate potential utility in a cellular context, we tested compounds 1, 2, and 3 in a cellular assay modified from a previously described method.<sup>3</sup> We infected HeLa cells with a modified vaccinia virus expressing ss-LEQLE-SIINFPEKL, an N-extended, ER-targeted variant of the ovalbumin-derived MHC-I binding model peptide epitope SIINFPEKL. Presentation of this peptide requires trimming by ERAP1.<sup>11</sup> We measured the amount of SIINFPEKL bound to MHC-I H-2 Kb at the cell surface using the monoclonal antibody 25D1, which specifically binds this particular MHC-peptide complex (Figure 9A). As a control for off-target effects, we used modified vaccinia virus expressing Ub-SIINFPEKL, a ubiquitinated construct where the SIINFPEKL peptide is generated in the cytosol by proteasomal processing. In this case, the processed peptide is transported to the ER by the transporter TAP1/2 for loading onto MHC-I, bypassing the need for ERAP1 processing.<sup>11</sup> Treatment of cells with the ERAP1 inhibitor leucinethiol (Leu-SH) inhibits 25D1 staining of cells infected with virus carrying ss-LEQLE-SIINFPEKL but has no effect on 25D1 staining of cells transfected with the ERAP1-independent construct Ub-SIINFPEKL (Figure 9B).

Using this approach, we evaluated the cellular efficacy of compounds 1, 2, and 3. HeLa cells treated with compound 1 at 50 μM exhibited reduced presentation of the 25D1 epitope derived from the control Ub-SIINFPEKL construct, indicative of an off-target (non-ERAP1) effect, such as alteration in peptide or MHC expression, peptide loading, or intracellular transport (Figure 9C). No further inhibition was observed for the ERAP1-dependent ss-LEQLE-SIINFPEKL construct, and cellular studies of compound 1 were not pursued further.

Compounds 2 and 3 exhibited specific inhibition of ERAP1 in the cellular context. For both compounds, significant inhibition of ERAP1 processing was observed for the 25D1

epitope derived from the ERAP1-dependent ss-LEQLE-SIINFPEKL construct, but no reduction was observed for the control Ub-SIINFPEKL construct (Figure 9C). The inhibition was dose-dependent, with compound 2 exhibiting an IC<sub>50</sub> value of 45 μM, and compound 3 exhibiting substantially higher potency with IC<sub>50</sub> of 1 μM (Figure 9D).

As an additional specificity test, we evaluated compound 21, an inactive derivative of compound 2 with *N*-phenylpiperazine replacing *N*-acetyl-piperazine, resulting in ~100-fold decrease in potency in biochemical L-AMC hydrolysis assay (Table 1). In the cellular assay, this compound also exhibited weaker potency than compound 2, with IC<sub>50</sub> > 500 μM. We attempted to similarly investigate compound 47, an inactive derivative of compound 3, wherein the benzoic acid moiety is converted to the methyl ester (Table 2). However, cells treated with compound 47 exhibited substantially reduced presentation in the Ub-SIINFPEKL control condition, indicative of an off-target inhibitory effect unrelated to ERAP1 and not observed with compound 3, and so could not be used for validation in this manner.

**Differential Efficacy of Compound 3 on ERAP1 Polymorphic Variants.** ERAP1 has several alleles present at high frequency in the human population, some of which correlate with susceptibility or resistance to autoimmune diseases such as ankylosing spondylitis.<sup>60</sup> To determine the ERAP1 polymorphic variants carried by the HeLa cell line used in Figure 9, we PCR-amplified and sequenced genomic DNA flanking known single nucleotide polymorphisms (SNPs)<sup>61</sup> and found that HeLa cells are heterozygous for two SNPs, 528R/K and 730Q/E, and homozygous for the other SNPs (see the Supporting Information). To investigate the effect of these polymorphisms on the potency of compound 3, we performed L-AMC hydrolysis assay as before, using recombinant ERAP1 variants corresponding to 5SNP, previously used for structural and enzymatic studies, and common naturally occurring alleles II and III (Figure 10A). Compound 3

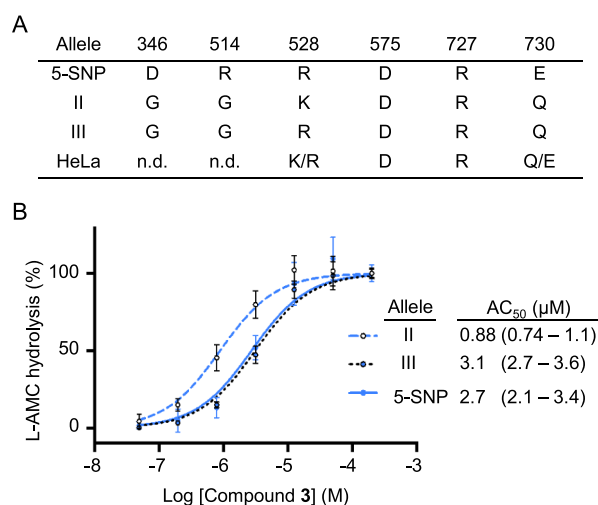


**Figure 10.** Compound 3 exhibits ERAP1 allele-dependent potency. ERAP1 hydrolysis activity of L-AMC was measured in two independent experiments, and data points were pooled, normalized, and fit with a sigmoidal curve. Reported are derived AC<sub>50</sub> with 95% confidence intervals, and the maximum activation observed for each allele relative to activity in the absence of the activator, expressed as a fraction of the baseline. Allele II AC<sub>50</sub> is significantly lower, \**p* < 0.0001 (extra sum-of-squares F test).

activates all three ERAP1 alleles under these conditions but is a more potent activator of disease-associated allele II, which it activates with sub-micromolar  $AC_{50}$  (Figure 10B). This difference likely is related to the polymorphic site at position 528, which is the only polymorphic position unique to allele II, where it is present as lysine relative to arginine in the other alleles.

## DISCUSSION

We implemented a high-throughput screen for short substrate inhibitors and activators of ERAP1. Counter-screens against ERAP2 and IRAP activity and cheminformatic filtering removed promiscuous compounds and identified three ERAP1-selective hit compounds. These all inhibited hydrolysis of a decamer peptide, similar in length to substrates that ERAP1 digests *in vivo*. Two compounds also inhibited ERAP1 activity in cellular assay. Docking sites were identified and validated through mechanism of action studies and by mutagenesis.

Compounds 1 and 2 were identified as novel non-peptidomimetic ERAP1-selective inhibitors that competitively inhibit ERAP1 activity, with predicted binding sites near the catalytic center overlapping with previously identified binding sites for peptidomimetic dipeptide and tripeptide substrate analogues (Figure 11). The highly conserved active site environment of oxytocinase subfamily members presents an interesting question of how these compounds maintain selectivity for ERAP1. Compound 1 is predicted by docking analysis to bind in a similar location as the nonspecific

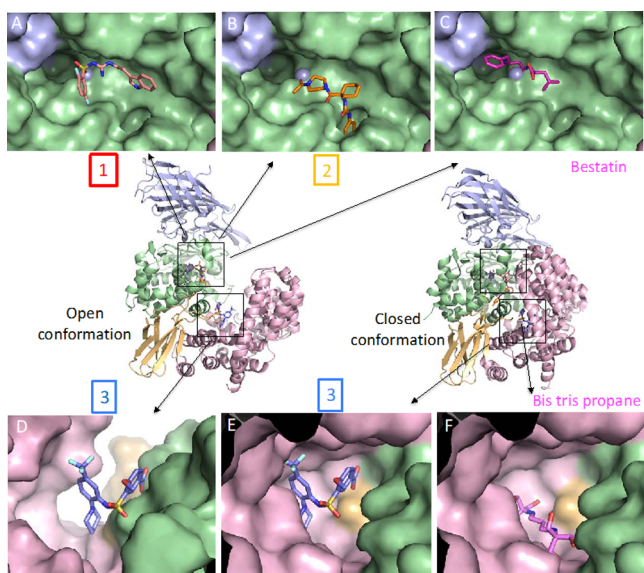


**Figure 11.** ERAP1 conformations and predicted inhibitor docking poses. Compounds 1 (A) and 2 (B) bind near the active site, shown for the open conformation. Interactions in the closed conformation are similar (not shown). The nonspecific aminopeptidase inhibitor bestatin (C) binds nearby. Compound 3 binds away from the active site at a domain interface, with different interactions in the open (D) and closed (E) conformations. In a recent high-resolution structure of ERAP1, a buffer component bis-tris-propane binds in a similar site (F). ERAP1 surface colored by the domain, with domain I in light blue, domain II in green, domain III in yellow, and domain IV in pink, with the active site Zn shown as a gray sphere. PDB 6MGQ (open) and 2YD0 (closed) were used for docking and ribbon representation. Bestatin is from PDB 2YD0 and bis-tris propane is from PDB 6Q4R.

aminopeptidase inhibitor bestatin, but its tryptamine moiety extends far beyond the bestatin's isoleucine side chain at the P1' position, accessing a small pocket lined by the ERAP1 specific residue T350A, and its difluorobenzene moiety binds a surface adjacent to the S1 site. The preferred docking pose for compound 2 places its cyclohexyl group in the same location as the compound 1 indole moiety, explaining the shared sensitivity to the ERAP1 mutation T350A, and its tolyl group in a deep pocket not accessed by bestatin (or other bound substrates).<sup>2,7,53,62</sup> This docking pose is supported by the observed SAR. Substitution of the *N*-acetyl piperazine moiety in compound 2, which is predicted to ligand the catalytic zinc through the *N*-acetyl oxygen, abrogates (compound 20) or greatly reduces (compound 21) the observed inhibition, with substitutions of the cyclohexyl and tolyl groups having minor effects consistent with disruption of hydrophobic interactions in the pockets noted above.

The discovery of compound 3 identifies the first nonpeptide small molecule that allosterically activates ERAP1 hydrolysis activity of L-AMC. The preferred docking pose for compound 3 places it far from the active site, at a junction between domains II, III, and IV (green, orange, and pink, respectively) near a site, where bis-tris-propane was found to bind in a recent high-resolution crystal structure of ERAP1 bound to a short peptidomimetic inhibitor.<sup>62</sup> SAR analysis supports this pose. Compound 3 required the aromatic carboxylic acid group for activation of ERAP1's L-AMC hydrolysis activity, as the methyl ester 47 was inactive (Table 2, Supporting Information, Figure S3). In the preferred docking pose, the carboxylate forms a salt bridge with Lys551 from domain II, and mutagenesis of this residue strongly reduces compound 3 inhibition (Figure 8). Based on the competitive mode of binding observed for compound 3 for full-length peptide substrates (Figure 5B) and the allosteric activation of ERAP1 by compound 3 observed for L-AMC and L-pNA (Figure 5A), it is attractive to speculate that compound 3 binds at a site also occupied by the C-terminal region of long-peptide substrates, as previously proposed for ERAP1 allosteric activation by short substrates<sup>2</sup> (Supporting Information Figure S1). This pose also provides a potential explanation for the discordant effects of compound 47 in L-AMC and WK10 peptide hydrolysis assays, where esterification of the aromatic carboxylic acid would interfere with interactions with domain II necessary for allosteric activation of L-AMC hydrolysis, while retaining interactions with domain IV necessary for the hypothesized C-terminal peptide docking. The C-terminal docking site for long ERAP1 peptide substrates has not yet been definitively identified, with a separate pocket in domain IV (near the alternate docking site for compound 3) proposed based on binding of maleic acid from the crystallization solution<sup>62</sup> and studies of peptide binding by isolated domain IV.<sup>7,63</sup> However, peptides might access different C-terminal binding sites<sup>62</sup> and the competitive nature of inhibition by compound 3 by long-peptide substrates does not preclude other modes of binding that do not involve a shared binding site.

Compound 3 is an aryl sulfonamide, which might be expected to bind to the active site zinc, as previously shown for other aryl sulfonamide inhibitors of zinc aminopeptidases including IRAP.<sup>55,56</sup> However, this mode of inhibition cannot explain the behavior observed for 3, as it activates hydrolysis of L-AMC, and therefore does not occlude the catalytic site. Very recently, a new small-molecule sulfonamide inhibitor (compound 6ad in Lee et al.)<sup>38</sup> has been identified for human

aminopeptidase N (CD13) and shown by X-ray crystallography to engage zinc through its hydroxamide rather than the sulfonamide moiety.<sup>38</sup>

Among the three hit compounds, activator **3** exhibits the highest potency for ERAP1 in all assays, including cellular assay. Screening small molecules for modulation of allosteric activation might be a promising strategy to identify inhibitors inaccessible by conventional short substrate inhibitor screens, particularly for enzymes that degrade biological polymers (proteases, glycosidases, and nucleases) likely to have extended substrate binding sites. Interestingly, the IC<sub>50</sub> observed for compound **3** was somewhat lower in cellular assay using an immunodominant MHC-I epitope than measured in biochemical assays using purified ERAP1 and either peptide or activated amino acid substrates (Supporting Information, Table S1). Further experimentation would be required to understand this behavior, but possible explanations include selective uptake of compound **3** by HeLa cells or the nonlinearity of the antigen loading process in vivo.

The inhibitory activity of compounds **2** and **3** in intracellular antigen processing assay suggests that these compounds could be used to probe the specific role of ERAP1 in vivo, similar to less-selective peptidomimetic compounds.<sup>12</sup> Lack of ERAP1 activity is known to elicit a cell-mediated immune response,<sup>9,64</sup> presumably by allowing presentation of antigenic peptides that are normally degraded by ERAP1, but the immunological and possible therapeutic relevance of transient specific inhibition is not well understood. For example, specific ERAP1 inhibition might modulate a mounting immune response by temporarily disrupting the MHC-I peptidome.<sup>12</sup> This disruption might impair a T-cell mediated response, which normally expands as T cells recognize a peptide antigen bound to MHC-I. Obscuring a peptide antigen in this manner by altering its trimming could be beneficial if this T-cell response has deleterious effects, such as in psoriasis<sup>65,66</sup> or ankylosing spondylitis.<sup>67</sup> M1 aminopeptidase inhibition has also been correlated with increased antitumor immune response, another potential field of interest.<sup>13,68</sup> ERAP1 expression is altered in malignancies of different tissue origins,<sup>69</sup> and in cases where ERAP1 overexpression protects cancerous cells from immune detection by degrading antigenic peptides, ERAP1 inhibition may produce a productive immune antitumor response. The physiological outcome (whether immunomodulation or immunostimulation) from specific ERAP1 inhibition remains unclear but discovery of these selective compounds will allow deeper investigation to proceed.<sup>48,70</sup>

## CONCLUSIONS

Three new compounds that specifically inhibit peptide hydrolysis by the ER-resident zinc aminopeptidase ERAP1 were identified and characterized. All are highly specific for ERAP1 over the homologous enzymes ERAP2 and IRAP. Two of the compounds (**2** and **3**) are active in a cellular context, inhibiting processing of a virally encoded antigenic peptide for presentation onto MHC-I molecules. One of the compounds (**3**) was identified originally as an activator of L-AMC hydrolysis but effectively inhibits processing of peptides with 8–13 residues, corresponding to the optimal lengths of physiologically relevant ERAP1 substrates. Based on docking and mutagenesis studies, compound **3** appears to act by an allosteric mechanism, binding at a site distant from the catalytic center accessible to long but not short substrates. Compounds **1** and **2** appear to dock in the active site and

inhibit ERAP1 by a competitive mechanism. Compound **3** discriminates between common variants of ERAP1, with submicromolar potency for a key disease-associated allele. We hope that these compounds may prove useful in continuing development of ERAP1-specific inhibitors for potential research and therapeutic applications.

## EXPERIMENTAL SECTION

**General Methods.** All reactions were performed under an inert atmosphere of dry argon or nitrogen either in a flame-dried or oven-dried glassware or in a glass microwave vial (Biotage, LLC). All anhydrous solvents were either purchased from Sigma-Aldrich or dried via passage through a glass contour solvent system (Pure Process Technology, LLC). All chemicals and reagents were purchased from TCI, Sigma-Aldrich, or Oakwood Products Inc.

Thin-layer chromatography (TLC) was performed using commercial aluminum-backed silica plates (TLC Silica gel 60 F-254, analytical chromatography). Visualization was accomplished with UV light. Flash column chromatography was performed using silica gel (230–400 mesh) or by reversed-phase flash chromatography on a CombiFlash purification system (50 g HP C18 Gold column). Nuclear magnetic resonance (NMR) spectra were recorded on either a 400 or 500 MHz Bruker AVANCE spectrometer with a dual carbon/proton cryoprobe. NMR spectra were recorded in deuterated chloroform or dimethyl sulfoxide. Chemical shifts are reported in parts per million (ppm) and are referenced to the center line of the solvent ( $\delta$  2.50 and 7.26 ppm with respect to dimethyl sulfoxide-*d*<sub>6</sub> and chloroform-*d* for <sup>1</sup>H NMR and  $\delta$  39.52 and 77.16 ppm with respect to dimethyl sulfoxide-*d*<sub>6</sub> and chloroform-*d* for <sup>13</sup>C NMR). Coupling constants are given in hertz (Hz). The spin multiplicities are reported as s = singlet, d = doublet, t = triplet, q = quartet, dd = doublet of doublet, td = doublet of triplet, and m = multiplet. NMR data analysis used MNova software. HRMS data were collected on an LCT Premier (Waters Corp., Milford MA) time-of-flight mass spectrometer.

The purity of final compounds was determined by analytical HPLC and was found to be  $\geq$ 95% pure. Analysis was performed on a Waters Acquity UPLC system equipped with a Waters Acquity photodiode array detector and a LCT premier TOF MS detector under the following conditions: column, Acquity BEH C18 (1.7  $\mu$ m, 2.1 mm  $\times$  50 mm); solvent A, H<sub>2</sub>O containing 0.05% formic acid; solvent B, CH<sub>3</sub>CN containing 0.05% formic acid; gradient, 5% B to 95% B over 5 min; flow rate, 0.6 mL/min. Purity data for target compounds are provided in the Experimental Section.

**N-(N-(2-(1H-Indol-3-yl)ethyl)carbamimidoyl)-2,5-difluorobenzenesulfonamide (1).** A mixture of tryptamine hydrochloride **4** (20 mg, 0.10 mmol) and 1H-pyrazole-1-carboximidamide hydrochloride **5** (18 mg, 0.12 mmol) in CH<sub>3</sub>CN (2 mL) was treated with DIEA (52  $\mu$ L, 0.30 mmol) under argon. The resulting reaction mixture was stirred at room temperature (23 °C) for 16–20 h; progress of the reaction was monitored by LC–MS. Solvent and other volatiles were removed under reduced pressure, and the residue was dried under high vacuum. The crude product **6** was dissolved in acetone (2 mL) and treated with 2,5-difluorobenzene sulfonyl chloride (21 mg, 0.10 mmol) and NaOH (8 mg, 0.20 mmol). The reaction mixture was stirred at room temperature for 12 h and then concentrated under reduced pressure. The residue was purified by reversed-phase flash chromatography, eluting with H<sub>2</sub>O and CH<sub>3</sub>CN both containing 0.1% TFA (90:10 to 10:90), to give compound **1** (13 mg, 35% yield over two steps) as a viscous oil. <sup>1</sup>H NMR (400 MHz, methanol-*d*<sub>4</sub>):  $\delta$  7.4 (ddd, *J* = 7.8, 5.4, 3.2 Hz, 1H), 7.4 (dt, *J* = 8.0, 1.0 Hz, 1H), 7.3–7.2 (m, 2H), 7.1 (td, *J* = 9.2, 4.1 Hz, 1H), 7.0 (ddd, *J* = 8.1, 7.0, 1.2 Hz, 1H), 7.0 (s, 1H), 6.9 (ddd, *J* = 8.0, 7.0, 1.0 Hz, 1H), 3.3 (t, *J* = 7.2 Hz, 2H), 2.9 (t, *J* = 7.2 Hz, 2H); <sup>13</sup>C NMR (101 MHz, methanol-*d*<sub>4</sub>):  $\delta$  162.0, 159.0 (dd, *J* = 245.4, 2.5 Hz), 156.0 (dd, *J* = 249.8, 2.7 Hz), 138.1, 128.3, 123.8, 122.3, 122.1 (dd, *J* = 24.5, 8.9 Hz), 119.6, 119.5 (dd, *J* = 24.7, 8.2 Hz), 119.0, 117.2 (d, *J* = 27.1 Hz), 112.3, 112.2, 44.7, 26.9; HRMS *m/z*: [M + H]<sup>+</sup> calcd for C<sub>17</sub>H<sub>17</sub>F<sub>2</sub>N<sub>4</sub>O<sub>2</sub>S, 379.1040; found, 379.1043. Purity > 99%.

**General Procedure for the Synthesis of Compound 2 and Analogues.** 1-(1-(4-Acetylpiperazine-1-carbonyl)cyclohexyl)-3-(*p*-tolyl)urea (**2**). A solution of amino acid **7** (143 mg, 1.0 mmol) in THF–H<sub>2</sub>O mixture (1:1) (8 mL) was treated with NaOH (80 mg, 2.0 mmol) and di-*tert*-butyl dicarbonate (262 mg, 1.2 mmol). The resulting reaction mixture was stirred at room temperature (23 °C) for 16 h; progress of the reaction monitored by TLC. Upon completion, the reaction mixture was concentrated to half the original volume, acidified to pH ≈ 2 using aqueous 1 N HCl, and extracted with CH<sub>2</sub>Cl<sub>2</sub>. The organic layer was dried over MgSO<sub>4</sub> and concentrated to yield the *N*-Boc-protected amino acid **8**.

The abovementioned crude product **8** (243 mg, 1.0 mmol) was dissolved in CH<sub>2</sub>Cl<sub>2</sub> (10 mL) and treated with HATU (570 mg, 1.5 mmol) and DIEA (0.35 mL, 2.0 mmol) under argon. The mixture was stirred for 10–15 min at room temperature and then treated with *N*-acetylpiperazine (256 mg, 2.0 mmol). After stirring at room temperature for 16 h, the reaction mixture was concentrated under reduced pressure. The residue was purified by flash chromatography on silica gel, eluting with CH<sub>2</sub>Cl<sub>2</sub> and MeOH (100:0 to 90:10), to yield intermediate **11** (265 mg, 75%) as a white solid.

A solution of compound **11** (35 mg, 0.10 mmol) from the abovementioned step in CH<sub>2</sub>Cl<sub>2</sub> (2 mL) was treated with TFA (1 mL) at room temperature. After stirring for 1 h, the reaction mixture was concentrated under reduced pressure, and the excess TFA was removed azeotropically with toluene. The crude product was dissolved in CH<sub>2</sub>Cl<sub>2</sub> (2 mL) and treated with DIEA (52 μL, 0.30 mmol) and *p*-tolyl isocyanate (20 mg, 0.15 mmol). The reaction mixture was stirred at room temperature for 8 h and then concentrated under reduced pressure. The residue was purified by reversed-phase flash chromatography, eluting with H<sub>2</sub>O and CH<sub>3</sub>CN both containing 0.1% TFA (90:10 to 10:90), to provide compound **2** (29 mg, 75% yield) as an off-white solid. <sup>1</sup>H NMR (400 MHz, DMSO-*d*<sub>6</sub>): δ 8.39 (s, 1H), 7.22 (d, *J* = 8.4 Hz, 2H), 7.02 (d, *J* = 8.2 Hz, 2H), 6.52 (s, 1H), 3.58 (broad s, 4H), 3.37–3.29 (m, 4H), 2.20 (s, 3H), 1.95 (s, 3H), 1.92 (broad s, 2H), 1.74–1.63 (m, 2H), 1.61–1.52 (m, 3H), 1.51–1.39 (m, 2H), 1.28–1.14 (m, 1H); <sup>13</sup>C NMR (101 MHz, DMSO-*d*<sub>6</sub>): δ 171.6, 168.3, 153.4, 137.6, 130.0, 129.1, 117.6, 57.7, 45.6, 40.8, 32.6, 24.9, 21.2, 21.0, 20.3; HRMS *m/z*: [M + H]<sup>+</sup> calcd for C<sub>21</sub>H<sub>31</sub>N<sub>4</sub>O<sub>3</sub>, 387.2396; found, 387.2390. Purity > 99%.

**General Procedure for the Synthesis of Compound 3 and Analogues.** 4-Methoxy-3-(*N*-(2-(piperidin-1-yl)-5-(trifluoromethyl)phenyl)sulfamoyl)benzoic Acid (**3**). A solution of 1-fluoro-2-nitro-4-(trifluoromethyl)benzene **24** (210 mg, 1.0 mmol) and piperidine (85 mg, 1.0 mmol) in DMF (6 mL) was treated with K<sub>2</sub>CO<sub>3</sub> (276 mg, 2.0 mmol). The resulting reaction mixture was heated at 120 °C for 6 h, cooled to room temperature, and extracted with EtOAc. The organic portion was washed with saturated aqueous NaCl solution, dried over MgSO<sub>4</sub>, and evaporated under reduced pressure. The residue was dissolved in EtOH (8 mL), SnCl<sub>2</sub>·2H<sub>2</sub>O (378 mg, 2.0 mmol) was added, and the mixture was heated at 70 °C for 1 h. The reaction mixture was cooled to ambient temperature, treated with saturated aqueous NaHCO<sub>3</sub> solution, and extracted with EtOAc (2×). The combined organic portion was washed with saturated aqueous NaCl solution, dried over MgSO<sub>4</sub>, filtered, and evaporated. The residue was purified by flash chromatography on silica gel, eluting with CH<sub>2</sub>Cl<sub>2</sub>/MeOH, to provide the aniline **32** (192 mg, 79%, over two steps) as an off-white solid.

Thionyl chloride (0.5 mL, excess) was added to 3-(chlorosulfonyl)-4-methoxybenzoic acid (25 mg, 0.10 mmol) under argon. The reaction mixture was stirred at room temperature for 16 h, quenched with methanol, and stirred for an additional 2 h. The reaction mixture was concentrated under reduced pressure, and the residue was dried under high vacuum for several hours to provide sulfonyl chloride **37**, which was used as such in the next reaction.

The substituted aniline **32** (24 mg, 0.10 mmol) and crude sulfonyl chloride **37** (25 mg, 0.10 mmol) were dissolved in pyridine (1 mL), and the resulting reaction mixture was stirred at room temperature for 12–16 h. Progress of the reaction was monitored by TLC, and upon completion, the reaction mixture was diluted with EtOAc and washed with aqueous 1 N HCl. The organic layer was dried over MgSO<sub>4</sub> and

concentrated to dryness. The residue was dissolved in the THF–H<sub>2</sub>O (1:1) (2 mL) mixture and treated with LiOH·H<sub>2</sub>O (10 mg, 0.24 mmol). The reaction mixture was stirred vigorously at room temperature for 6–8 h. Solvents were removed under reduced pressure, and the residue was purified by reversed-phase flash chromatography, eluting with H<sub>2</sub>O and CH<sub>3</sub>CN (both containing 0.1% TFA), to provide compound **3** (16 mg, 35% over two steps) as a solid. <sup>1</sup>H NMR (500 MHz, DMSO-*d*<sub>6</sub>): δ 13.20 (s, 1H), 8.77 (s, 1H), 8.36 (d, *J* = 2.2 Hz, 1H), 8.15 (dd, *J* = 8.7, 2.2 Hz, 1H), 7.44 (d, *J* = 2.0 Hz, 1H), 7.38–7.29 (m, 3H), 3.92 (s, 3H), 2.82–2.72 (m, 4H), 1.73–1.62 (m, 4H), 1.59–1.50 (m, 2H); <sup>13</sup>C NMR (126 MHz, DMSO-*d*<sub>6</sub>): δ 165.7, 159.4, 147.5, 136.7, 132.1, 131.5, 125.7, 124.2 (q, *J* = 32.1 Hz), 123.9 (q, *J* = 270.4 Hz), 122.9, 122.0, 121.4 (d, *J* = 4.1 Hz), 114.7 (q, *J* = 3.9 Hz), 113.4, 57.0, 52.6, 25.8, 23.4; <sup>19</sup>F NMR (471 MHz, DMSO-*d*<sub>6</sub>): δ –61.1; HRMS *m/z*: [M + H]<sup>+</sup> calcd for C<sub>20</sub>H<sub>22</sub>F<sub>3</sub>N<sub>2</sub>O<sub>5</sub>S, 459.1202; found, 459. Purity > 99%.

1-(1-(4-Acetylpiperazine-1-carbonyl)cyclohexyl)-3-(4-chlorophenyl)urea (**16**). The title compound was synthesized following the general procedure described above for compound **2**. Off-white solid (8 mg, 73% yield). <sup>1</sup>H NMR (400 MHz, DMSO-*d*<sub>6</sub>): δ 8.63 (s, 1H), 7.37 (d, *J* = 9.1 Hz, 2H), 7.26 (d, *J* = 9.1 Hz, 2H), 6.62 (s, 1H), 3.59 (broad s, 4H), 3.42–3.28 (m, 4H), 1.96 (s, 3H), 1.92 (s, 2H), 1.68 (t, *J* = 13.6 Hz, 2H), 1.62–1.52 (m, 3H), 1.51–1.37 (m, 2H), 1.30–1.12 (m, 1H); <sup>13</sup>C NMR (101 MHz, DMSO-*d*<sub>6</sub>): δ 171.5, 168.3, 153.1, 139.1, 128.6, 124.7, 119.0, 57.7, 45.6, 40.8, 32.5, 24.9, 21.2, 21.0; HRMS *m/z*: [M + H]<sup>+</sup> calcd for C<sub>20</sub>H<sub>28</sub>ClN<sub>4</sub>O<sub>3</sub>, 407.1850; found, 407.1843.

1-(1-(4-Acetylpiperazine-1-carbonyl)cyclohexyl)-3-(4-methoxyphenyl)urea (**17**). The title compound was synthesized following the general procedure described above for compound **2**. Off-white solid (25 mg, 65% yield). <sup>1</sup>H NMR (400 MHz, DMSO-*d*<sub>6</sub>): δ 8.33 (s, 1H), 7.26 (d, *J* = 9.0 Hz, 2H), 6.82 (d, *J* = 9.2 Hz, 2H), 6.49 (s, 1H), 3.70 (s, 3H), 3.59 (broad s, 4H), 3.39–3.31 (m, 4H), 1.97 (s, 3H), 1.93 (broad s, 2H), 1.69 (t, *J* = 11.9 Hz, 2H), 1.62–1.52 (m, 3H), 1.51–1.39 (m, 2H), 1.29–1.13 (m, 1H); <sup>13</sup>C NMR (101 MHz, DMSO-*d*<sub>6</sub>): δ 171.7, 168.3, 154.0, 153.5, 133.2, 119.1, 113.9, 57.6, 55.1, 45.6, 32.6, 28.8, 24.9, 21.1, 21.0; HRMS *m/z*: [M + H]<sup>+</sup> calcd for C<sub>21</sub>H<sub>31</sub>N<sub>4</sub>O<sub>4</sub>, 403.2345; found, 403.2352.

1-(1-(4-Acetylpiperazine-1-carbonyl)cyclohexyl)-3-(4-fluorophenyl)urea (**18**). The title compound was synthesized following the general procedure described above for compound **2**. Off-white solid (20 mg, 71% yield). <sup>1</sup>H NMR (400 MHz, methanol-*d*<sub>4</sub>): δ 7.37–7.29 (m, 2H), 7.02–6.95 (m, 2H), 3.76 (broad s, 4H), 3.58–3.47 (m, 4H), 2.15–2.03 (m, 5H), 1.93–1.80 (m, 2H), 1.76–1.49 (m, 5H), 1.41–1.25 (m, 1H); <sup>13</sup>C NMR (101 MHz, methanol-*d*<sub>4</sub>): δ 174.8, 171.9, 159.9 (d, *J* = 240 Hz), 156.0, 136.7, 121.8 (d, *J* = 7.6 Hz), 116.3 (d, *J* = 22.6 Hz), 59.9, 47.2, 42.6, 34.2, 26.3, 22.5, 21.1; HRMS *m/z*: [M + H]<sup>+</sup> calcd for C<sub>20</sub>H<sub>28</sub>FN<sub>4</sub>O<sub>3</sub>, 391.2145; found, 391.2147.

1-(1-(4-Acetylpiperazine-1-carbonyl)cyclohexyl)-3-phenylurea (**19**). The title compound was synthesized following the general procedure described above for compound **2**. Off-white solid (35 mg, 70% yield). <sup>1</sup>H NMR (400 MHz, methanol-*d*<sub>4</sub>): δ 7.37–7.29 (m, 2H), 7.29–7.18 (m, 2H), 7.01–6.92 (m, 1H), 3.77 (broad s, 4H), 3.59–3.46 (m, 4H), 2.10 (s, 2H), 2.07 (s, 3H), 1.93–1.79 (m, 2H), 1.74–1.64 (m, 3H), 1.63–1.50 (m, 2H), 1.41–1.25 (m, 1H); <sup>13</sup>C NMR (101 MHz, MeOD-*d*<sub>4</sub>): δ 174.8, 171.9, 156.0, 140.6, 129.9, 123.6, 119.9, 59.9, 47.2, 42.5, 34.2, 26.3, 22.5, 21.1; HRMS *m/z*: [M + H]<sup>+</sup> calcd for C<sub>20</sub>H<sub>29</sub>N<sub>4</sub>O<sub>3</sub>, 373.2240; found, 373.2242.

1-(1-(Morpholine-4-carbonyl)cyclohexyl)-3-(*p*-tolyl)urea (**20**). The title compound was synthesized following the general procedure described above for compound **2**. Off-white solid (18 mg, 68% yield). <sup>1</sup>H NMR (400 MHz, DMSO-*d*<sub>6</sub>): δ 8.34 (s, 1H), 7.24 (d, *J* = 8.3 Hz, 2H), 7.03 (d, *J* = 8.3 Hz, 2H), 6.48 (s, 1H), 3.57 (s, 4H), 3.50–3.42 (m, 4H), 2.21 (s, 3H), 1.93 (d, *J* = 13.5 Hz, 2H), 1.75–1.61 (m, 2H), 1.61–1.51 (m, 3H), 1.50–1.36 (m, 2H), 1.27–1.12 (m, 1H); <sup>13</sup>C NMR (101 MHz, DMSO-*d*<sub>6</sub>): δ 171.5, 153.3, 137.6, 129.9, 129.1, 117.6, 66.1, 57.6, 40.4, 32.6, 24.9, 21.0, 20.3; HRMS *m/z*: [M + H]<sup>+</sup> calcd for C<sub>19</sub>H<sub>28</sub>N<sub>3</sub>O<sub>3</sub>, 346.2131; found, 346.2138.

**1-(1-(4-Phenylpiperazine-1-carbonyl)cyclohexyl)-3-(p-tolyl)urea (21).** The title compound was synthesized following the general procedure described above for compound 2. Off-white solid (20 mg, 68% yield).  $^1\text{H NMR}$  (400 MHz,  $\text{DMSO}-d_6$ ):  $\delta$  7.25–7.13 (m, 4H), 6.99 (d,  $J = 8.1$  Hz, 2H), 6.86 (d,  $J = 8.2$  Hz, 2H), 6.76 (t,  $J = 7.2$  Hz, 1H), 3.73 (s, 4H), 3.12–2.96 (m, 4H), 2.18 (s, 3H), 1.97 (d,  $J = 13.4$  Hz, 2H), 1.79–1.65 (m, 2H), 1.63–1.40 (m, 5H), 1.32–1.12 (m, 1H);  $^{13}\text{C NMR}$  (101 MHz,  $\text{DMSO}-d_6$ ):  $\delta$  171.4, 153.3, 150.8, 137.5, 129.9, 129.0, 128.8, 119.1, 117.6, 117.5, 115.6, 57.6, 48.5, 32.6, 24.9, 21.0, 20.2; HRMS  $m/z$ :  $[\text{M} + \text{H}]^+$  calcd for  $\text{C}_{25}\text{H}_{33}\text{N}_4\text{O}_2$ , 421.2604; found, 421.2607.

**1-(1-(4-Acetylpiperazin-1-yl)-2-methyl-1-oxopropan-2-yl)-3-(p-tolyl)urea (22).** The title compound was synthesized following the general procedure described above for compound 2. Off-white solid (22 mg, 67% yield).  $^1\text{H NMR}$  (400 MHz,  $\text{DMSO}-d_6$ ):  $\delta$  8.28 (s, 1H), 7.22 (d,  $J = 8.3$  Hz, 2H), 7.01 (d,  $J = 8.3$  Hz, 2H), 6.63 (s, 1H), 3.58 (s, 4H), 3.42–3.28 (m, 4H), 2.20 (s, 3H), 1.96 (s, 3H), 1.39 (s, 6H);  $^{13}\text{C NMR}$  (101 MHz,  $\text{DMSO}-d_6$ ):  $\delta$  171.3, 168.3, 153.8, 137.6, 130.0, 129.0, 117.8, 55.5, 45.6, 40.8, 40.4, 26.5, 21.2, 20.3; HRMS  $m/z$ :  $[\text{M} + \text{H}]^+$  calcd for  $\text{C}_{18}\text{H}_{27}\text{N}_3\text{O}_3$ , 347.2083; found, 347.2080.

**1-(1-(4-Acetylpiperazine-1-carbonyl)cyclopropyl)-3-(p-tolyl)urea (23).** The title compound was synthesized following the general procedure described above for compound 2. Off-white solid (13 mg, 60% yield).  $^1\text{H NMR}$  (400 MHz,  $\text{DMSO}-d_6$ ):  $\delta$  8.18 (s, 1H), 7.24 (d,  $J = 8.2$  Hz, 2H), 7.09 (s, 1H), 7.02 (d,  $J = 8.2$  Hz, 2H), 3.65–3.47 (m, 4H), 3.45–3.35 (m, 4H), 2.21 (s, 3H), 2.00 (s, 3H), 1.25–1.14 (m, 2H), 1.00–0.86 (m, 2H);  $^{13}\text{C NMR}$  (101 MHz,  $\text{DMSO}-d_6$ ):  $\delta$  169.4, 168.5, 154.9, 154.8, 137.3, 130.3, 129.0, 118.1, 118.0, 45.5, 34.6, 21.2, 20.2, 13.9; HRMS  $m/z$ :  $[\text{M} + \text{H}]^+$  calcd for  $\text{C}_{18}\text{H}_{23}\text{N}_4\text{O}_3$ , 345.1927; found, 345.1928.

**4-Chloro-3-(N-(2-(piperidin-1-yl)-5-(trifluoromethyl)phenyl)sulfamoyl)benzoic Acid (41).** The title compound was synthesized following the general procedure described above for compound 3. Viscous oil (20 mg, 32% yield).  $^1\text{H NMR}$  (500 MHz,  $\text{DMSO}-d_6$ ):  $\delta$  8.44 (s, 1H), 8.13 (d,  $J = 8.0$  Hz, 1H), 7.82 (d,  $J = 8.2$  Hz, 1H), 7.44 (d,  $J = 7.7$  Hz, 1H), 7.35 (s, 1H), 7.30 (d,  $J = 8.4$  Hz, 1H), 2.75 (broad s, 4H), 1.54 (broad s, 4H), 1.46 (broad s, 2H);  $^{13}\text{C NMR}$  (126 MHz,  $\text{DMSO}-d_6$ ):  $\delta$  165.6, 150.3, 137.7, 135.5, 135.4, 133.2, 131.9, 131.4, 130.7, 125.4, 124.3 (q,  $J = 271.6$  Hz), 123.4, 122.6, 119.2, 53.0, 25.9, 23.8;  $^{19}\text{F NMR}$  (471 MHz,  $\text{DMSO}-d_6$ ):  $\delta$  -60.9; HRMS  $m/z$ :  $[\text{M} + \text{H}]^+$  calcd for  $\text{C}_{19}\text{H}_{19}\text{ClF}_3\text{N}_2\text{O}_4\text{S}$ , 463.0706; found, 463.0712.

**4-Bromo-3-(N-(2-(piperidin-1-yl)-5-(trifluoromethyl)phenyl)sulfamoyl)benzoic Acid (42).** The title compound was synthesized following the general procedure described above for compound 3. Off-white solid (15 mg, 20% yield).  $^1\text{H NMR}$  (500 MHz,  $\text{DMSO}-d_6$ ):  $\delta$  8.53–8.46 (s, 1H), 8.05–7.95 (m, 2H), 7.45–7.25 (m, 3H), 2.82–2.68 (broad s, 4H), 1.65–1.52 (broad s, 4H), 1.51–1.40 (broad s, 2H);  $^{13}\text{C NMR}$  (126 MHz,  $\text{DMSO}-d_6$ ):  $\delta$  165.8, 149.4, 139.1, 136.8, 135.2, 132.1, 131.6, 131.3, 124.5, 124.3 (q,  $J = 271.5$  Hz), 123.2, 123.0, 122.6, 117.9, 53.0, 25.9, 23.8;  $^{19}\text{F NMR}$  (471 MHz,  $\text{DMSO}-d_6$ ):  $\delta$  -61.1; HRMS  $m/z$ :  $[\text{M} + \text{H}]^+$  calcd for  $\text{C}_{19}\text{H}_{19}\text{BrF}_3\text{N}_2\text{O}_4\text{S}$ , 507.0201; found, 507.0205.

**3-(N-(2-(Piperidin-1-yl)-5-(trifluoromethyl)phenyl)sulfamoyl)benzoic Acid (43).** The title compound was synthesized following the general procedure described above for compound 3. Solid (45 mg, 30% yield).  $^1\text{H NMR}$  (500 MHz,  $\text{DMSO}-d_6$ ):  $\delta$  8.38 (s, 1H), 8.08 (d,  $J = 7.7$  Hz, 1H), 7.79 (d,  $J = 7.8$  Hz, 1H), 7.48 (t,  $J = 7.6$  Hz, 1H), 7.40 (s, 1H), 7.22 (d,  $J = 8.5$  Hz, 1H), 7.08 (d,  $J = 8.2$  Hz, 1H), 2.69 (broad s, 4H), 1.57 (broad s, 4H), 1.44 (broad s, 2H);  $^{13}\text{C NMR}$  (126 MHz,  $\text{DMSO}-d_6$ ):  $\delta$  167.9, 149.7, 141.9, 139.5, 135.0, 133.1, 128.6, 128.0, 127.6, 124.8 (q,  $J = 271.5$  Hz), 123.6, 123.3, 120.9, 118.3, 52.5, 25.9, 24.1;  $^{19}\text{F NMR}$  (471 MHz,  $\text{DMSO}-d_6$ ):  $\delta$  -60.5; HRMS  $m/z$ :  $[\text{M} + \text{H}]^+$  calcd for  $\text{C}_{19}\text{H}_{20}\text{F}_3\text{N}_2\text{O}_4\text{S}$ , 429.1096; found, 429.1098.

**4-Methoxy-3-(N-(5-methyl-2-(piperidin-1-yl)phenyl)sulfamoyl)benzoic Acid (44).** The title compound was synthesized following the general procedure described above for compound 3. Solid (23 mg, 20% yield).  $^1\text{H NMR}$  (500 MHz,  $\text{DMSO}-d_6$ ):  $\delta$  13.20 (s, 1H), 8.56 (s, 1H), 8.38 (d,  $J = 2.2$  Hz, 1H), 8.13 (dd,  $J = 8.7, 2.2$  Hz, 1H), 7.30

(d,  $J = 8.8$  Hz, 1H), 7.13–7.05 (m, 2H), 6.81–6.74 (m, 1H), 3.95 (s, 3H), 2.63–2.60 (m, 4H), 2.12 (s, 3H), 1.70–1.63 (m, 4H), 1.53 (broad s, 2H);  $^{13}\text{C NMR}$  (126 MHz,  $\text{DMSO}-d_6$ ):  $\delta$  165.8, 159.4, 140.3, 136.5, 134.3, 132.0, 131.6, 125.7, 124.4, 122.7, 121.8, 116.5, 113.4, 57.1, 53.5, 26.4, 23.4, 20.9; HRMS  $m/z$ :  $[\text{M} + \text{H}]^+$  calcd for  $\text{C}_{20}\text{H}_{25}\text{N}_2\text{O}_5\text{S}$ , 405.1484; found, 405.1479.

**3-(N-(5-Fluoro-2-(piperidin-1-yl)phenyl)sulfamoyl)-4-methoxybenzoic Acid (45).** The title compound was synthesized following the general procedure described above for compound 3. Solid (35 mg, 33% yield).  $^1\text{H NMR}$  (500 MHz,  $\text{DMSO}-d_6$ ):  $\delta$  13.26 (s, 1H), 8.74 (s, 1H), 8.38 (d,  $J = 2.2$  Hz, 1H), 8.16 (dd,  $J = 8.7, 2.2$  Hz, 1H), 7.33 (d,  $J = 8.8$  Hz, 1H), 7.29 (dd,  $J = 8.8, 5.8$  Hz, 1H), 7.04 (dd,  $J = 10.6, 3.0$  Hz, 1H), 6.82 (td,  $J = 8.6, 3.0$  Hz, 1H), 3.97 (s, 3H), 2.66–2.61 (m, 4H), 1.72–1.64 (m, 4H), 1.53 (s, 2H);  $^{13}\text{C NMR}$  (126 MHz,  $\text{DMSO}-d_6$ ):  $\delta$  165.7, 159.4, 158.9 (d,  $J = 240.8$  Hz), 139.0 (d,  $J = 2.7$  Hz), 136.8, 133.7 (d,  $J = 11.4$  Hz), 131.5, 125.4, 124.0, 123.9 (d,  $J = 9.8$  Hz), 113.6, 110.0 (d,  $J = 22.0$  Hz), 103.1 (d,  $J = 28.0$  Hz), 57.2, 53.5, 26.3, 23.4; HRMS  $m/z$ :  $[\text{M} + \text{H}]^+$  calcd for  $\text{C}_{19}\text{H}_{22}\text{FN}_2\text{O}_5\text{S}$ , 409.1233; found, 409.1238.

**4-Methoxy-3-(N-(2-(piperidin-1-yl)phenyl)sulfamoyl)benzoic Acid (46).** The title compound was synthesized following the general procedure described above for compound 3. Solid (45 mg, 30% yield).  $^1\text{H NMR}$  (500 MHz,  $\text{DMSO}-d_6$ ):  $\delta$  13.22 (s, 1H), 8.60 (s, 1H), 8.38 (d,  $J = 2.2$  Hz, 1H), 8.13 (dd,  $J = 8.7, 2.2$  Hz, 1H), 7.30 (d,  $J = 8.8$  Hz, 1H), 7.26–7.19 (m, 2H), 7.02–6.94 (m, 2H), 3.96 (s, 3H), 2.71–2.64 (m, 4H), 1.72–1.65 (m, 4H), 1.57–1.50 (m, 2H);  $^{13}\text{C NMR}$  (126 MHz,  $\text{DMSO}-d_6$ ):  $\delta$  165.8, 159.4, 142.9, 136.5, 132.1, 131.6, 125.8, 125.1, 123.9, 122.8, 121.9, 116.0, 113.4, 57.1, 53.3, 26.3, 23.5; HRMS  $m/z$ :  $[\text{M} + \text{H}]^+$  calcd for  $\text{C}_{19}\text{H}_{23}\text{N}_2\text{O}_5\text{S}$ , 391.1328; found, 391.1332.

**Methyl 4-Methoxy-3-(N-(2-(piperidin-1-yl)-5-(trifluoromethyl)phenyl)sulfamoyl)benzoate (47).** The title compound was synthesized following the general procedure described above for compound 3. Viscous oil (25 mg, 30% yield).  $^1\text{H NMR}$  (500 MHz,  $\text{DMSO}-d_6$ ):  $\delta$  8.80 (s, 1H), 8.36 (s, 1H), 8.18 (d,  $J = 8.7$  Hz, 1H), 7.44 (s, 1H), 7.39–7.29 (m, 3H), 3.93 (s, 3H), 3.85 (s, 3H), 2.76 (broad s, 4H), 1.65 (broad s, 4H), 1.53 (broad s, 2H);  $^{13}\text{C NMR}$  (126 MHz,  $\text{DMSO}-d_6$ ):  $\delta$  165.1, 160.2, 154.9, 148.2, 137.0, 135.2, 132.4, 131.7, 126.5, 124.9 (q,  $J = 271.5$  Hz), 122.5, 122.0, 115.6 (q,  $J = 4$  Hz), 114.1, 57.5, 53.0, 52.8, 26.2, 23.9;  $^{19}\text{F NMR}$  (471 MHz,  $\text{DMSO}-d_6$ ):  $\delta$  -61.1; HRMS  $m/z$ :  $[\text{M} + \text{H}]^+$  calcd for  $\text{C}_{21}\text{H}_{24}\text{F}_3\text{N}_2\text{O}_5\text{S}$ , 473.1358; found, 473.1363.

**4-Methoxy-3-(N-methyl-N-(2-(piperidin-1-yl)-5-(trifluoromethyl)phenyl)sulfamoyl)benzoic Acid (49).** The title compound was synthesized by treating compound 47 (46 mg, 0.10 mmol) with NaH (6.5 mg, 0.15 mmol) and methyl iodide (0.075 mL, 0.12 mmol) in DMF (2 mL) at room temperature for 18 h. The methyl ester was hydrolyzed using the method described above for compound 3 and afforded compound 49 (13 mg, 25% yield over two steps) as a viscous oil.  $^1\text{H NMR}$  (500 MHz,  $\text{DMSO}-d_6$ ):  $\delta$  8.25–8.19 (m, 2H), 7.53 (d,  $J = 8.4$  Hz, 1H), 7.44 (d,  $J = 9.3$  Hz, 1H), 7.20 (d,  $J = 8.6$  Hz, 1H), 7.01 (s, 1H), 3.99 (s, 3H), 3.28 (s, 3H), 3.06 (broad s, 4H), 1.60 (broad s, 4H), 1.53 (broad s, 2H);  $^{13}\text{C NMR}$  (126 MHz,  $\text{DMSO}-d_6$ ):  $\delta$  166.3, 160.1, 154.2, 136.7, 134.3, 132.5, 128.1, 126.0, 125.5, 124.4 (q,  $J = 271.0$  Hz), 123.6, 123.3, 121.8, 114.0, 57.1, 51.9, 37.9, 26.1, 24.2;  $^{19}\text{F NMR}$  (471 MHz,  $\text{DMSO}-d_6$ ):  $\delta$  -60.5; HRMS  $m/z$ :  $[\text{M} + \text{H}]^+$  calcd for  $\text{C}_{21}\text{H}_{24}\text{F}_3\text{N}_2\text{O}_5\text{S}$ , 473.1358; found, 473.1355.

**4-Methoxy-3-(N-(2-(4-methylpiperazin-1-yl)-5-(trifluoromethyl)phenyl)sulfamoyl)benzoic Acid (50).** The title compound was synthesized following the general procedure described above for compound 3. Solid (10 mg, 25% yield).  $^1\text{H NMR}$  (500 MHz,  $\text{DMSO}-d_6$ ):  $\delta$  8.36 (s, 1H), 7.97 (d,  $J = 8.5$  Hz, 1H), 7.44 (s, 1H), 7.11 (s, 2H), 7.01 (d,  $J = 8.6$  Hz, 1H), 3.77 (s, 3H), 2.85 (broad s, 4H), 2.48–2.40 (broad s, 4H), 2.20 (s, 3H);  $^{13}\text{C NMR}$  (126 MHz,  $\text{DMSO}-d_6$ ):  $\delta$  163.4, 159.4, 144.4, 135.3, 134.2, 130.7, 127.2, 126.1, 124.0 (q,  $J = 272$  Hz), 123.9, 122.5, 120.6, 116.1, 112.2, 55.8, 53.2, 48.4, 42.3;  $^{19}\text{F NMR}$  (471 MHz,  $\text{DMSO}-d_6$ ):  $\delta$  -60.6; HRMS  $m/z$ :  $[\text{M} + \text{H}]^+$  calcd for  $\text{C}_{20}\text{H}_{23}\text{F}_3\text{N}_3\text{O}_5\text{S}$ , 474.1311; found, 474.1315.

**Protein Expression and Purification.** Human ERAP1, human ERAP2, and mouse IRAP were expressed recombinantly by

baculoviral infection of High Five (BTA-TN-SB1-4) *Trichoplusia ni* insect cells grown in SFX serum-free media (Hyclone). ERAP1 corresponds to UniProtKB Q9NZ08 with three different sets of allelic variants (see Figure 10B). ERAP2 corresponds to UniProtKB Q6P179 with Asn392. IRAP corresponds to the luminal domain of UniProtKB Q8C129. Expression constructs for ERAP1, ERAP2, and IRAP contain the endogenous signal sequences for ER translocation and an additional C-terminal 6xHis tag. Three days after infection by mixing cells ( $7 \times 10^5$  cells per mL) with 1% (v/v) virus preparation, the culture supernatant was collected by centrifugation and concentrated and buffer exchanged >100-fold into binding buffer (50 mM phosphate pH 8.0, 300 mM NaCl, 10 mM imidazole). After filtration, His-tagged protein was captured and eluted from Ni-nitilotriacetate-agarose resin (Qiagen) in buffer containing 100 mM imidazole. Enzyme stocks were characterized by sodium dodecyl sulfate (SDS)-polyacrylamide gel electrophoresis, and by measuring L-AMC (Acros Organics) hydrolysis by ERAP1 and IRAP, or R-AMC (Sigma-Aldrich) hydrolysis activity by ERAP2.

**MLPCN Library Screen.** HTS reaction conditions were 7  $\mu$ L per well in 1536-well plate format. Reactions were carried out using 20 mM Tris pH 7.5, 100 mM NaCl, 0.01% (w/v) bovine serum albumin (BSA), 0.4% (v/v) DMSO, 1 ng/ $\mu$ L enzyme, and 10.7  $\mu$ M substrate. After mixing, plates were incubated for 1 h at room temperature, and then, fluorescence emission was measured at 450 nm with 380 nm excitation. Z'-scores ranged from 0.8 to 0.94, using 100  $\mu$ M leucine-thiol (Sigma-Aldrich) as a positive control for inhibition.

**Fluorogenic and Chromogenic Amino Acid Hydrolysis Assays.** For fluorogenic amino acids L-AMC and R-AMC assays, reactions were carried out in 100  $\mu$ L per well in black flat-bottom 96-well polypropylene plates (Greiner Bio-One) in 20 mM Tris-HCl pH 7.5, 100 mM NaCl, 0.01% (w/v) BSA. Enzyme (400 ng ERAP1, 12.5 ng ERAP2 or 40 ng IRAP per well) and hit compounds (200–0.012  $\mu$ M, 4-fold dilutions were used) were mixed, and then, substrate (final concentration 100  $\mu$ M L-AMC for ERAP1 and IRAP, 10  $\mu$ M R-AMC for ERAP2) was added to start the reaction. Fluorescence at 380/460 nm was measured using a BMG POLARstar OPTIMA once every 10 min starting after addition of the substrate. Reaction rates were quantified by calculating the rate of fluorescence change. Each plate contained controls with DMSO alone, or with 100  $\mu$ M each leucine-thiol and DTT. All reactions were normalized using these two conditions as 100 and 0% activity, respectively. To half-maximal inhibitory or activating concentrations, normalized data points were fit with a sigmoidal curve constrained to 100% (top) for inhibitors or 100% (bottom) for activators. ERAP1 allelic variants were tested and analyzed identically.

**Peptide Hydrolysis Assay.** For measurement of peptide hydrolysis using mass spectrometry, reactions were carried out in 50  $\mu$ L volumes in 96 well V-bottom plate format with 20 mM Tris-HCl pH 7.5, 100 mM NaCl, 0.01% (w/v) BSA. Purified ERAP1 (20 ng/well) and hit compounds (200–0.048  $\mu$ M, 4-fold dilutions) were mixed, and then, the substrate peptide (WRCYEKMALK, 10  $\mu$ M final concentration, synthesized by 21st Century Biochemicals) was added to start the reaction. After 10 min, the reaction was stopped by addition of 25  $\mu$ L 1.2% TFA. Product peptide (RCYEKMALK) was quantified using RapidFire LC-MS (Agilent, Pure Honey Technologies) by summing the area under the curve. Each plate contained controls with DMSO alone, or with TFA stop solution added prior to adding ERAP1. All reactions were normalized using these two conditions as 100 and 0% activity, respectively. IC<sub>50</sub> was determined by fitting normalized data points with a sigmoidal curve constrained to 100% (top) for inhibitors or 100% (bottom) for activators.

For measurements of peptide hydrolysis using coupled enzyme assay, ERAP1 (400 ng/well) and compound 3 (0–25  $\mu$ M, 2-fold dilutions) were mixed, and then, the substrate LF9 peptide (LVAFKARKF)<sup>5</sup> at a series of concentrations (160–1.25  $\mu$ M, 2-fold dilutions) along with 25  $\mu$ L of coupling reagent was added to start the reaction. The coupling reagent (25  $\mu$ L) consisted 131.7 ng 2,2'-azino-bis(3-ethylbenzthiazoline-6-sulfonic acid) (ABTS, Sigma), 15 ng horseradish peroxidase (HRP, Sigma), and 21 ng L-amino acid oxidase (Sigma) in 20 mM Tris-HCl pH 7.5, 100 mM NaCl and is

prepared 10 min before starting the reaction. In this assay, the N-terminal Leu released from LF9 peptide upon hydrolysis by ERAP1 is oxidized by L-amino acid oxidase to  $\alpha$ -ketoisocaproic acid, releasing hydrogen peroxide which is a substrate for HRP. HRP uses the hydrogen peroxide to oxidize ABTS that absorbs at 405 nm. After starting the reaction, absorbance at 405 nm was measured once every 2.5 min for 20 min. Reaction rates were quantified by calculating the rate of absorbance change over the time course, which was linear under these conditions. Michaelis–Menten analysis was performed by fitting the slopes as function of substrate concentration in standard Michaelis–Menten equation using GraphPad Prism using the equation,  $Y = V_{\max}X/(K_m + X)$ , where Y is the initial reaction rate,  $V_{\max}$  is the maximum enzyme velocity, X is the substrate concentration, and  $K_m$  is the substrate concentration needed to achieve half maximum enzyme velocity.

**Enzyme Inhibitor Mode of Action Studies.** For mode of action studies, enzyme kinetics experiments were performed by measuring the rate of hydrolysis of the L-leucine-p-nitroanilide (L-pNA), a chromogenic substrate, at different substrate concentrations in the absence and presence of compounds 1 (200–3.125  $\mu$ M, 4-fold dilution), 2 (25–3.125  $\mu$ M, 2-fold dilution), and 3 (12–0.195  $\mu$ M, 4-fold dilution) under same assay conditions as L-AMC hydrolysis. L-pNA was used rather than L-AMC to allow for investigation of a range of substrate concentrations that would be precluded by inner filter and fluorescence quenching effects in fluorescence assay. The measurements were performed on the BMG POLARstar OPTIMA plate reader, and initial reaction rates were calculated for all substrate concentrations from slopes obtained over a time course of 5–10 min. Initial rates were fit to an allosteric (cooperative) sigmoid model, using GraphPad Prism software, according to the equation  $Y = (V_{\max}X^h)/(K_{\text{prime}} + X^h)$ , where X is the substrate concentration, Y is the initial reaction rate,  $V_{\max}$  is the reaction rate at infinite time, and h is the Hill coefficient.  $K_{\text{prime}}$  is a parameter related to  $K_m$  and is calculated with the equation  $K_{\text{prime}} = K_{\text{half}}^h$ , where  $K_{\text{half}}$  is the concentration of the substrate that produces a half-maximal enzyme velocity. For competitive mode of action of inhibitors 1 and 2, the complete data set of initial rates of L-pNA hydrolysis at different inhibitor concentrations were fit to a competitive allosteric inhibition model, using GraphPad Prism software using the equation  $Y = V_{\max}X^h/(K_{\text{half}}^h(1 + I^h/K_i^h) + X^h)$ , where I is inhibitor concentration and  $K_i$  is the inhibition constant, while Y, h,  $K_{\text{prime}}$ ,  $K_{\text{half}}$  and  $V_{\max}$  are the same as described for the allosteric sigmoidal model. For mode of action of analysis of compound 3 (25–1.56  $\mu$ M, 2-fold dilution), the complete data set of slopes and substrate concentrations for the LF9 peptide (160–1.25  $\mu$ M, 2-fold dilutions) hydrolysis reaction in the presence and absence of the inhibitor were fit to competitive inhibition equation using GraphPad Prism,  $Y = V_{\max}X/(K_m\text{Obs} + X)$ , where  $K_m\text{Obs} = K_m(1 + [I]/K_i)$ , I is inhibitor concentration, and  $K_i$  is the inhibition constant, while Y, X,  $V_{\max}$  and  $K_m$  are the same as described before.

**In Silico Docking.** Compound structures with appropriate geometry were generated initially using the PRODRG server.<sup>71</sup> Docking simulations and energy minimization was performed using Schrödinger Maestro software package.<sup>72</sup> Compound structures were prepared for docking using LigPrep (pH 7.5  $\pm$  0.5) and docked using Glide onto either a closed structure of ERAP1 allele II based on PDB ID 2YD0<sup>53</sup> or an open structure of ERAP1 allele IV based on PDB ID 6MGQ which were both prepared for ligand docking using Prime. A search volume encompassing the entire enclosed surface of ERAP1 concurrent with the active site was used (ligand diameter midpoint search volume 40 Å  $\times$  40 Å  $\times$  40 Å). Compounds 1 and 2 were docked without any excluded volume. Compound 3 docking enforced a 6 Å spherical exclusion volume centered on the active-site zinc atom, as this compound is known to activate short substrate hydrolysis; therefore, the active site is likely not occluded upon binding of compound 3. Docking solutions were then inspected, and one solution per compound was selected for further energy minimization using Embrace, using the OPLS3 force field, PRCG method, 2500 maximum iterations, converge on gradient, a convergence threshold of 0.05, and the energy difference mode.

**Cellular Antigen Processing Assay.** HeLa cells stably expressing H-2 K<sup>b</sup> were grown to 90% confluency in 24 well plates and infected with recombinant vaccinia virus containing a cassette to express the ovalbumin epitope SIINFEKL at the C-terminus of ubiquitin or a cassette which contains the same epitope preceded by an ER translocation signal sequence and the sequence LEQLE, which are immediately N-terminal to the SIINFEKL epitope in the ovalbumin sequence. Both viral strains also express GFP with an IRES translation start site in frame with the SIINFEKL epitope. At the time of infection, cells were treated with the inhibitor. After 16–24 h, the cells were pipetted off the plate and stained with 25D1 antibody specific for SIINFEKL in complex with H-2 K<sup>b</sup>, followed by Alexa Fluor 647-goat anti mouse secondary antibody (Thermo Fisher). Cells were then fixed in 4% formalin and analyzed by flow cytometry by gating on singlet GFP+ population and quantifying Alexa 647 median fluorescence intensity. Two experiments used 10-fold dilutions of inhibitors (50  $\mu$ M, 5  $\mu$ M, 500 nM, 50 nM, and 5 nM), and one experiment used 2-fold dilutions in the relevant region (50, 25, 12.5, 6.25, 3.125  $\mu$ M).

The ERAP1 polymorphisms carried by the HeLa cell line were determined by DNA sequencing of PCR amplicons surrounding the polymorphic sites. HeLa cells were washed twice with ice-cold PBS, and the cell lysates were digested overnight at 55 °C with lysis buffer [10 mM NaCl, 10 mM Tris-HCl pH 7.5, 10 mM ethylenediaminetetraacetate (EDTA), 0.5% SDS and 0.4 mg/mL PK]. Genomic DNA was subjected to phenol/CHCl<sub>3</sub> extraction and followed precipitation with 1/10 vol of 3 M NaOAc and 2 vol of 100% EtOH. After a wash with 70% EtOH, genomic DNA was resuspended in 10 mM Tris-HCl 5 mM EDTA pH 8.0 and its concentration and purification were tested by NanoDrop. Each DNA sample (100 ng) was used as the template for conventional PCR. Forward and reverse primers (5' to 3') are AAATGGGTGATGTGTCTGCC & TCAAAAG-CAAGGTTCCATCC for exon 10, CATGATAGGTGATTTAA-TAACTGCTTG & TTTTCACATTCCTCCTTGAATTAAC for exon 11, and TACTGGTCCCTGTTTCCCTG & AACAGAAAA-GATGCCCTTCA for exon 14. The PCR products were sent for sequencing to VBC Biotech in Austria.

**Data Analysis.** Data fitting was performed using Graphpad Prism 7.<sup>73</sup> Structural modeling data were analyzed, and figures were prepared using PyMOL.<sup>74</sup>

## ■ ASSOCIATED CONTENT

### 📄 Supporting Information

The Supporting Information is available free of charge at <https://pubs.acs.org/doi/10.1021/acs.jmedchem.9b00293>.

Schematic diagrams, structure–activity relationships, alternate docking poses, L-pNA hydrolysis activity, validation of docking sites, flow cytometry, kinetic parameters, EC<sub>50</sub> values, and <sup>1</sup>H NMR and <sup>13</sup>C NMR spectra of compounds 1–3, 16–23, and 41–50 (PDF)

Molecular formula strings (CSV)

## ■ AUTHOR INFORMATION

### Corresponding Author

\*E-mail: [Lawrence.Stern@umassmed.edu](mailto:Lawrence.Stern@umassmed.edu). Phone: 508-856-1831. Fax: 508-856-0019.

### ORCID

Akbar Ali: 0000-0003-3491-791X

Efstratios Stratikos: 0000-0002-3566-2309

Jennifer Golden: 0000-0002-6813-3710

Lawrence J. Stern: 0000-0001-9870-8557

### Present Addresses

<sup>#</sup>San Francisco State University, 1600 Holloway Avenue, San Francisco, California 94132, United States.

<sup>¶</sup>INSERM U1149, Hôpital Bichat, Xavier Bichat Medical University, 16 rue H Huchard, 75018 Paris, France.

<sup>∇</sup>University of Wisconsin, 777 Highland Avenue, Madison, Wisconsin 53705, United States.

## Author Contributions

Z.M., R.A., and D.R. contributed equally to this work. T.T.N., I.E., E.S., and L.J.S. planned and performed preliminary screening using LOPAC 1280 library. Z.M., R.S., and L.J.S. planned MLPCN screen. W.F.A., S.M., M.H., S.B., and R.S. optimized, performed, and analyzed MLPCN screen, dose-dependent confirmation, and counter-screens. J.G. guided SAR studies. D.R. performed synthetic chemistry and characterized all compounds. Z.M. and R.A. expressed and purified proteins and performed peptide and amino-acid substrate IC<sub>50</sub> assays. Z.M. performed peptide hydrolysis assays, in silico docking, and cellular inhibition experiments. R.A. performed mechanism of action studies and designed and analyzed mutant ERAP1 proteins. Z.M., R.A., and L.J.S. planned experiments and interpreted data. Z.M., R.A., D.R., A.A., and L.J.S. wrote the manuscript. All authors have given approval to the final version of the manuscript.

## Funding

This work was supported by grants from the NIH Molecular Library Probe Center Network MLPCN (R03MH097543) (L.J.S.) and NIAID (R01AI038996) (L.J.S.). I.E. was supported by a short-term EMBO fellowship. E.S. acknowledges funding by the European Union (European Social Fund) and Greek national funds through the Operational Program “Education and Lifelong Learning” of the National Strategic Reference Framework: Research Funding Program of the General Secretariat for Research & Technology (grant nos. LS7-2199 and ERC-14).

## Notes

The authors declare no competing financial interest.

## ■ ACKNOWLEDGMENTS

HeLa-expressing H-2 Kb, 25D1 cells for antibody production, and vaccinia virus strains were generously provided by Dr. Kenneth Rock (UMMS). Preliminary screening experiments were performed with the assistance of the UMMS Chemical Screening Facility. The HTS data are submitted as PubChem AID 652221, “Broad Institute Small Molecule Probes of ERAP-1 Inhibitor Probe Project”. We are grateful to Patti M. Aha and Catherine Communal for assistance in organization and coordination of this collaborative effort and for assistance in submitting findings to PubChem. The authors thank Dr. Alexandros Petropoulos for sequencing the ERAP1 gene in HeLa cells. The cell-based assay used for this research was derived from a HeLa cell line. Henrietta Lacks, and the HeLa cell line that was established from her tumor cells without her knowledge or consent in 1951, has made significant contributions to scientific progress and advances in human health. We are grateful to Henrietta Lacks, now deceased, and to her surviving family members for their contributions to biomedical research.

## ■ ABBREVIATIONS

DIEA, *N,N*-diisopropylethylamine; DMF, dimethylformamide; ER, endoplasmic reticulum; ERAP1, endoplasmic reticulum aminopeptidase 1; ERAP2, endoplasmic reticulum aminopeptidase 2; HATU, 1-[bis(dimethylamino)-methylene]-1*H*-1,2,3-triazolo[4,5-*b*]pyridinium 3-oxid hexafluorophosphate;



IRAP, insulin-regulated aminopeptidase; L-AMC, leucine-7-amido-4-methylcoumarin;  $AC_{50}$ , half-maximal activating concentration;  $EC_{50}$ , half-maximal effective concentration;  $IC_{50}$ , half-maximal inhibitory concentration; BSA, bovine specific albumin; Ni-NTA, nickel-nitrilotriacetate; SNP, single-nucleotide polymorphism; TFA, trifluoroacetic acid

## REFERENCES

- (1) Serwold, T.; Gonzalez, F.; Kim, J.; Jacob, R.; Shastri, N. ERAAP customizes peptides for MHC class I molecules in the endoplasmic reticulum. *Nature* **2002**, *419*, 480–483.
- (2) Nguyen, T. T.; Chang, S.-C.; Evnouchidou, I.; York, I. A.; Zikos, C.; Rock, K. L.; Goldberg, A. L.; Stratikos, E.; Stern, L. J. Structural basis for antigenic peptide precursor processing by the endoplasmic reticulum aminopeptidase ERAP1. *Nat. Struct. Mol. Biol.* **2011**, *18*, 604–613.
- (3) York, I. A.; Chang, S.-C.; Saric, T.; Keys, J. A.; Favreau, J. M.; Goldberg, A. L.; Rock, K. L. The ER aminopeptidase ERAP1 enhances or limits antigen presentation by trimming epitopes to 8-9 residues. *Nat. Immunol.* **2002**, *3*, 1177–1184.
- (4) Chang, S.-C.; Momburg, F.; Bhutani, N.; Goldberg, A. L. The ER aminopeptidase, ERAP1, trims precursors to lengths of MHC class I peptides by a “molecular ruler” mechanism. *Proc. Natl. Acad. Sci. U.S.A.* **2005**, *102*, 17107–17112.
- (5) Evnouchidou, I.; Momburg, F.; Papakyriakou, A.; Chroni, A.; Leondiadis, L.; Chang, S.-C.; Goldberg, A. L.; Stratikos, E. The internal sequence of the peptide-substrate determines its N-terminus trimming by ERAP1. *PLoS One* **2008**, *3*, No. e3658.
- (6) Zervoudi, E.; Papakyriakou, A.; Georgiadou, D.; Evnouchidou, I.; Gajda, A.; Poreba, M.; Salvesen, G. S.; Drag, M.; Hattori, A.; Swevers, L.; Vourloumis, D.; Stratikos, E. Probing the S1 specificity pocket of the aminopeptidases that generate antigenic peptides. *Biochem. J.* **2011**, *435*, 411–420.
- (7) Gandhi, A.; Lakshminarasimhan, D.; Sun, Y.; Guo, H. C. Structural insights into the molecular ruler mechanism of the endoplasmic reticulum aminopeptidase ERAP1. *Sci. Rep.* **2011**, *1*, 186.
- (8) Węglarz-Tomczak, E.; Vassiliou, S.; Mucha, A. Discovery of potent and selective inhibitors of human aminopeptidases ERAP1 and ERAP2 by screening libraries of phosphorus-containing amino acid and dipeptide analogues. *Bioorg. Med. Chem. Lett.* **2016**, *26*, 4122–4126.
- (9) Hammer, G. E.; Gonzalez, F.; James, E.; Nolla, H.; Shastri, N. In the absence of aminopeptidase ERAAP, MHC class I molecules present many unstable and highly immunogenic peptides. *Nat. Immunol.* **2007**, *8*, 101–108.
- (10) Nagarajan, N. A.; de Verteuil, D. A.; Sriranganadane, D.; Yahyaoui, W.; Thibault, P.; Perreault, C.; Shastri, N. ERAAP shapes the peptidome associated with classical and nonclassical MHC class I molecules. *J. Immunol.* **2016**, *197*, 1035–1043.
- (11) York, I. A.; Brehm, M. A.; Zendzian, S.; Towne, C. F.; Rock, K. L. Endoplasmic reticulum aminopeptidase 1 (ERAP1) trims MHC class I-presented peptides in vivo and plays an important role in immunodominance. *Proc. Natl. Acad. Sci. U.S.A.* **2006**, *103*, 9202–9207.
- (12) Koumantou, D.; Barnea, E.; Martin-Esteban, A.; Maben, Z.; Papakyriakou, A.; Mpakali, A.; Kokkala, P.; Pratsinis, H.; Georgiadis, D.; Stern, L. J.; Admon, A.; Stratikos, E. Editing the immunopeptidome of melanoma cells using a potent inhibitor of endoplasmic reticulum aminopeptidase 1 (ERAP1). *Cancer Immunol. Immunother.* **2019**, *68*, 1245–1261.
- (13) James, E.; Bailey, I.; Sugiyarto, G.; Elliott, T. Induction of protective antitumor immunity through attenuation of ERAAP function. *J. Immunol.* **2013**, *190*, 5839–5846.
- (14) de Castro, J. A. L.; Alvarez-Navarro, C.; Brito, A.; Guasp, P.; Martín-Esteban, A.; Sanz-Bravo, A. Molecular and pathogenic effects of endoplasmic reticulum aminopeptidases ERAP1 and ERAP2 in MHC-I-associated inflammatory disorders: Towards a unifying view. *Mol. Immunol.* **2016**, *77*, 193–204.
- (15) Mehta, A. M.; Jordanova, E. S.; Corver, W. E.; van Wezel, T.; Uh, H.-W.; Kenter, G. G.; Jan Fleuren, G. Single nucleotide polymorphisms in antigen processing machinery component ERAP1 significantly associate with clinical outcome in cervical carcinoma. *Genes Chromosomes Cancer* **2009**, *48*, 410–418.
- (16) Mehta, A. M.; Jordanova, E. S.; van Wezel, T.; Uh, H.-W.; Corver, W. E.; Kwappenberg, K. M. C.; Verduijn, W.; Kenter, G. G.; van der Burg, S. H.; Fleuren, G. J. Genetic variation of antigen processing machinery components and association with cervical carcinoma. *Genes Chromosomes Cancer* **2007**, *46*, 577–586.
- (17) Hisatsune, C.; Ebisui, E.; Usui, M.; Ogawa, N.; Suzuki, A.; Mataga, N.; Takahashi-Iwanaga, H.; Mikoshiba, K. ERp44 exerts redox-dependent control of blood pressure at the ER. *Mol. Cell* **2015**, *58*, 1015–1027.
- (18) Yamamoto, N.; Nakayama, J.; Yamakawa-Kobayashi, K.; Hamaguchi, H.; Miyazaki, R.; Arinami, T. Identification of 33 polymorphisms in the adipocyte-derived leucine aminopeptidase (ALAP) gene and possible association with hypertension. *Hum. Mutat.* **2002**, *19*, 251–257.
- (19) Hattori, A.; Kitatani, K.; Matsumoto, H.; Miyazawa, S.; Rogi, T.; Tsuruoka, N.; Mizutani, S.; Natori, Y.; Tsujimoto, M. Characterization of recombinant human adipocyte-derived leucine aminopeptidase expressed in Chinese hamster ovary cells. *J. Biochem.* **2000**, *128*, 755–762.
- (20) Georgiadou, D.; Hearn, A.; Evnouchidou, I.; Chroni, A.; Leondiadis, L.; York, I. A.; Rock, K. L.; Stratikos, E. Placental leucine aminopeptidase efficiently generates mature antigenic peptides in vitro but in patterns distinct from endoplasmic reticulum aminopeptidase 1. *J. Immunol.* **2010**, *185*, 1584–1592.
- (21) Saveanu, L.; Carroll, O.; Weimershaus, M.; Guernonprez, P.; Firat, E.; Lindo, V.; Greer, F.; Davoust, J.; Kratzer, R.; Keller, S. R.; Niedermann, G.; van Endert, P. IRAP identifies an endosomal compartment required for MHC class I cross-presentation. *Science* **2009**, *325*, 213–217.
- (22) Diwakarla, S.; Nylander, E.; Grönbladh, A.; Vanga, S. R.; Khan, Y. S.; Gutiérrez-de-Terán, H.; Ng, L.; Pham, V.; Sävmarker, J.; Lundbäck, T.; Jenmalm-Jensen, A.; Andersson, H.; Engen, K.; Rosenström, U.; Larhed, M.; Åqvist, J.; Chai, S. Y.; Hallberg, M. Binding to and inhibition of insulin-regulated aminopeptidase by macrocyclic disulfides enhances spine density. *Mol. Pharmacol.* **2016**, *89*, 413–424.
- (23) Niwa, M.; Numaguchi, Y.; Ishii, M.; Kuwahata, T.; Kondo, M.; Shibata, R.; Miyata, K.; Oike, Y.; Murohara, T. IRAP deficiency attenuates diet-induced obesity in mice through increased energy expenditure. *Biochem. Biophys. Res. Commun.* **2015**, *457*, 12–18.
- (24) Park, B. M.; Cha, S. A.; Han, B. R.; Kim, S. H. Angiotensin IV stimulates high atrial stretch-induced ANP secretion via insulin regulated aminopeptidase. *Peptides* **2015**, *63*, 30–37.
- (25) Hammer, G. E.; Gonzalez, F.; Champsaur, M.; Cado, D.; Shastri, N. The aminopeptidase ERAAP shapes the peptide repertoire displayed by major histocompatibility complex class I molecules. *Nat. Immunol.* **2006**, *7*, 103–112.
- (26) Serwold, T.; Gaw, S.; Shastri, N. ER aminopeptidases generate a unique pool of peptides for MHC class I molecules. *Nat. Immunol.* **2001**, *2*, 644–651.
- (27) Umezawa, H.; Aoyagi, T.; Suda, H.; Hamada, M.; Takeuchi, T. Bestatin, an inhibitor of aminopeptidase B, produced by actinomycetes. *J. Antibiot.* **1976**, *29*, 97–99.
- (28) Aoyagi, T.; Tobe, H.; Kojima, F.; Hamada, M.; Takeuchi, T.; Umezawa, H. Amastatin, an inhibitor of aminopeptidase A, produced by actinomycetes. *J. Antibiot.* **1978**, *31*, 636–638.
- (29) Stratikos, E.; Stern, L. J. Antigenic peptide trimming by ER aminopeptidases—insights from structural studies. *Mol. Immunol.* **2013**, *55*, 212–219.
- (30) Taylor, A.; Peltier, C. Z.; Torre, F. J.; Hakamian, N. Inhibition of bovine lens leucine aminopeptidase by bestatin: number of binding sites and slow binding of this inhibitor. *Biochemistry* **1993**, *32*, 784–790.

- (31) Wilkes, S. H.; Prescott, J. M. The slow, tight binding of bestatin and amastatin to aminopeptidases. *J. Biol. Chem.* **1985**, *260*, 13154–13162.
- (32) Chan, W. W.-C. L-leucinthiol - a potent inhibitor of leucine aminopeptidase. *Biochem. Biophys. Res. Commun.* **1983**, *116*, 297–302.
- (33) Bienvenue, D. L.; Bennett, B.; Holz, R. C. Inhibition of the aminopeptidase from *Aeromonas proteolytica* by L-leucinethiol: kinetic and spectroscopic characterization of a slow, tight-binding inhibitor-enzyme complex. *J. Inorg. Biochem.* **2000**, *78*, 43–54.
- (34) Huntington, K. M.; Bienvenue, D. L.; Wei, Y.; Bennett, B.; Holz, R. C.; Pei, D. Slow-binding inhibition of the aminopeptidase from *Aeromonas proteolytica* by peptide thiols: synthesis and spectroscopic characterization. *Biochemistry* **1999**, *38*, 15587–15596.
- (35) Papakyriakou, A.; Zervoudi, E.; Theodorakis, E. A.; Saveanu, L.; Stratikos, E.; Vourloumis, D. Novel selective inhibitors of aminopeptidases that generate antigenic peptides. *Bioorg. Med. Chem. Lett.* **2013**, *23*, 4832–4836.
- (36) Stamogiannos, A.; Papakyriakou, A.; Mauvais, F.-X.; van Endert, P.; Stratikos, E. Screening identifies thimerosal as a selective inhibitor of endoplasmic reticulum aminopeptidase 1. *ACS Med. Chem. Lett.* **2016**, *7*, 681–685.
- (37) Vanga, S. R.; Sävmarker, J.; Ng, L.; Larhed, M.; Hallberg, M.; Åqvist, J.; Hallberg, A.; Chai, S. Y.; Gutiérrez-de-Terán, H. Structural basis of inhibition of human insulin-regulated aminopeptidase (IRAP) by aryl sulfonamides. *ACS Omega* **2018**, *3*, 4509–4521.
- (38) Lee, J.; Vinh, N. B.; Drinkwater, N.; Yang, W.; Kannan Sivaraman, K.; Schembri, L. S.; Gazdik, M.; Grin, P. M.; Butler, G. S.; Overall, C. M.; Charman, S. A.; McGowan, S.; Scammells, P. J. Novel human aminopeptidase N inhibitors: discovery and optimization of subsite binding interactions. *J. Med. Chem.* **2019**, *62*, 7185–7209.
- (39) Bounaadja, L.; Schmitt, M.; Albrecht, S.; Mouray, E.; Tarnus, C.; Florent, I. Selective inhibition of PfA-M1, over PfA-M17, by an amino-benzosuberone derivative blocks malaria parasites development in vitro and in vivo. *Malar. J.* **2017**, *16*, 382.
- (40) Flipo, M.; Beghyn, T.; Leroux, V.; Florent, I.; Deprez, B. P.; Deprez-Poulain, R. F. Novel selective inhibitors of the zinc plasmodial aminopeptidase PfA-M1 as potential antimalarial agents. *J. Med. Chem.* **2007**, *50*, 1322–1334.
- (41) Cunningham, E.; Drag, M.; Kafarski, P.; Bell, A. Chemical target validation studies of aminopeptidase in malaria parasites using alpha-aminoalkylphosphonate and phosphonopeptide inhibitors. *Antimicrob. Agents Chemother.* **2008**, *52*, 3221–3228.
- (42) Dive, V.; Georgiadis, D.; Matziari, M.; Makaritis, A.; Beau, F.; Cuniasse, P.; Yiotakis, A. Phosphinic peptides as zinc metalloproteinase inhibitors. *Cell. Mol. Life Sci.* **2004**, *61*, 2010–2019.
- (43) Georgiadis, D.; Vazeux, G.; Llorens-Cortes, C.; Yiotakis, A.; Dive, V. Potent and selective inhibition of zinc aminopeptidase A (EC 3.4.11.7, APA) by glutamyl aminophosphinic peptides: importance of glutamyl aminophosphinic residue in the P1 position. *Biochemistry* **2000**, *39*, 1152–1155.
- (44) Kokkala, P.; Mpakali, A.; Mauvais, F.-X.; Papakyriakou, A.; Daskalaki, I.; Petropoulou, I.; Kavvalou, S.; Papathanasopoulou, M.; Agrotis, S.; Fonsou, T.-M.; van Endert, P.; Stratikos, E.; Georgiadis, D. Optimization and structure-activity relationships of phosphinic pseudotriptide inhibitors of aminopeptidases that generate antigenic peptides. *J. Med. Chem.* **2016**, *59*, 9107–9123.
- (45) Lejczak, B.; Kafarski, P.; Zygmunt, J. Inhibition of aminopeptidases by aminophosphonates. *Biochemistry* **1989**, *28*, 3549–3555.
- (46) Guzanov, P. ERAP1 inhibitor development. Ph.D. Thesis, Linacre College, Oxford University, Oxford, United Kingdom, 2017.
- (47) Evnouchidou, I.; Kamal, R. P.; Seregin, S. S.; Goto, Y.; Tsujimoto, M.; Hattori, A.; Voulgari, P. V.; Drosos, A. A.; Amalfitano, A.; York, I. A.; Stratikos, E. Cutting Edge: Coding single nucleotide polymorphisms of endoplasmic reticulum aminopeptidase 1 can affect antigenic peptide generation in vitro by influencing basic enzymatic properties of the enzyme. *J. Immunol.* **2011**, *186*, 1909–1913.
- (48) Drinkwater, N.; Lee, J.; Yang, W.; Malcolm, T. R.; McGowan, S. M1 aminopeptidases as drug targets: broad applications or therapeutic niche? *FEBS J.* **2017**, *284*, 1473–1488.
- (49) Georgiadis, D.; Mpakali, A.; Koumantou, D.; Stratikos, E. Inhibitors of ER aminopeptidase 1 and 2: from design to clinical application. *Curr. Med. Chem.* **2018**, *26*, 2715–2729.
- (50) Hattori, A.; Matsumoto, H.; Mizutani, S.; Tsujimoto, M. Molecular cloning of adipocyte-derived leucine aminopeptidase highly related to placental leucine aminopeptidase/oxytocinase. *J. Biochem.* **1999**, *125*, 931–938.
- (51) Evnouchidou, I.; Berardi, M. J.; Stratikos, E. A continuous fluorogenic assay for the measurement of the activity of endoplasmic reticulum aminopeptidase 1: competition kinetics as a tool for enzyme specificity investigation. *Anal. Biochem.* **2009**, *395*, 33–40.
- (52) Evnouchidou, I.; Papakyriakou, A.; Stratikos, E. A new role for Zn(II) aminopeptidases: antigenic peptide generation and destruction. *Curr. Pharm. Des.* **2009**, *15*, 3656–3670.
- (53) Kochan, G.; Krojer, T.; Harvey, D.; Fischer, R.; Chen, L.; Vollmar, M.; von Delft, F.; Kavanagh, K. L.; Brown, M. A.; Bowness, P.; Wordsworth, P.; Kessler, B. M.; Oppermann, U. Crystal structures of the endoplasmic reticulum aminopeptidase-1 (ERAP1) reveal the molecular basis for N-terminal peptide trimming. *Proc. Natl. Acad. Sci. U.S.A.* **2011**, *108*, 7745–7750.
- (54) Stamogiannos, A.; Maben, Z.; Papakyriakou, A.; Mpakali, A.; Kokkala, P.; Georgiadis, D.; Stern, L. J.; Stratikos, E. Critical role of interdomain interactions in the conformational change and catalytic mechanism of endoplasmic reticulum aminopeptidase 1. *Biochemistry* **2017**, *56*, 1546–1558.
- (55) Borhade, S. R.; Rosenström, U.; Sävmarker, J.; Lundbäck, T.; Jenmalm-Jensen, A.; Sigmundsson, K.; Axelsson, H.; Svensson, F.; Konda, V.; Sköld, C.; Larhed, M.; Hallberg, M. Inhibition of insulin-regulated aminopeptidase (IRAP) by arylsulfonamides. *ChemistryOpen* **2014**, *3*, 256–263.
- (56) Diwakarla, S.; Nylander, E.; Grönbladh, A.; Vanga, S. R.; Khan, Y. S.; Gutiérrez-de-Terán, H.; Sävmarker, J.; Ng, L.; Pham, V.; Lundbäck, T.; Jenmalm-Jensen, A.; Svensson, R.; Artursson, P.; Zellerroth, S.; Engen, K.; Rosenström, U.; Larhed, M.; Åqvist, J.; Chai, S. Y.; Hallberg, M. Aryl sulfonamide inhibitors of insulin-regulated aminopeptidase enhance spine density in primary hippocampal neuron cultures. *ACS Chem. Neurosci.* **2016**, *7*, 1383–1392.
- (57) Laskowski, R. A.; Swindells, M. B. LigPlot+: multiple ligand-protein interaction diagrams for drug discovery. *J. Chem. Inf. Model.* **2011**, *51*, 2778–2786.
- (58) Maret, W.; Li, Y. Coordination dynamics of zinc in proteins. *Chem. Rev.* **2009**, *109*, 4682–4707.
- (59) Amin, S. A.; Adhikari, N.; Jha, T. Design of Aminopeptidase N Inhibitors as Anti-cancer Agents. *J. Med. Chem.* **2018**, *61*, 6468–6490.
- (60) Roberts, A. R.; Appleton, L. H.; Cortes, A.; Vecellio, M.; Lau, J.; Watts, L.; Brown, M. A.; Wordsworth, P. ERAP1 association with ankylosing spondylitis is attributable to common genotypes rather than rare haplotype combinations. *Proc. Natl. Acad. Sci. U.S.A.* **2017**, *114*, 558–561.
- (61) Reeves, E.; Edwards, C. J.; Elliott, T.; James, E. Naturally occurring ERAP1 haplotypes encode functionally distinct alleles with fine substrate specificity. *J. Immunol.* **2013**, *191*, 35–43.
- (62) Giastas, P.; Neu, M.; Rowland, P.; Stratikos, E. High-resolution crystal structure of endoplasmic reticulum aminopeptidase 1 with bound phosphinic transition-state analogue inhibitor. *ACS Med. Chem. Lett.* **2019**, *10*, 708–713.
- (63) Sui, L.; Gandhi, A.; Guo, H.-C. Crystal structure of a polypeptide's C-terminus in complex with the regulatory domain of ER aminopeptidase 1. *Mol. Immunol.* **2016**, *80*, 41–49.
- (64) Nagarajan, N. A.; Gonzalez, F.; Shastri, N. Nonclassical MHC class Ib-restricted cytotoxic T cells monitor antigen processing in the endoplasmic reticulum. *Nat. Immunol.* **2012**, *13*, 579–586.
- (65) Di Meglio, P.; Duarte, J. H. CD8 T Cells and IFN-gamma emerge as critical players for psoriasis in a novel model of mouse psoriasisform skin inflammation. *J. Invest. Dermatol.* **2013**, *133*, 871–874.

(66) Di Meglio, P.; Villanova, F.; Navarini, A. A.; Mylonas, A.; Tosi, I.; Nestle, F. O.; Conrad, C. Targeting CD8(+) T cells prevents psoriasis development. *J. Allergy Clin. Immunol.* **2016**, *138*, 274–276.e6.

(67) Atagunduz, P.; Appel, H.; Kuon, W.; Wu, P.; Thiel, A.; Kloetzel, P.-M.; Sieper, J. HLA-B27-restricted CD8+ T cell response to cartilage-derived self peptides in ankylosing spondylitis. *Arthritis Rheum.* **2005**, *52*, 892–901.

(68) Keller, M.; Ebstein, F.; Bürger, E.; Textoris-Taube, K.; Gorny, X.; Urban, S.; Zhao, F.; Dannenberg, T.; Sucker, A.; Keller, C.; Saveanu, L.; Krüger, E.; Rothkötter, H.-J.; Dahlmann, B.; Henklein, P.; Voigt, A.; Kuckelkorn, U.; Paschen, A.; Kloetzel, P.-M.; Seifert, U. The proteasome immunosubunits, PA28 and ER-aminopeptidase 1 protect melanoma cells from efficient MART-126-35 -specific T-cell recognition. *Eur. J. Immunol.* **2015**, *45*, 3257–3268.

(69) Cifaldi, L.; Romania, P.; Lorenzi, S.; Locatelli, F.; Fruci, D. Role of endoplasmic reticulum aminopeptidases in health and disease: from infection to cancer. *Int. J. Mol. Sci.* **2012**, *13*, 8338–8352.

(70) Stratikos, E. Regulating adaptive immune responses using small molecule modulators of aminopeptidases that process antigenic peptides. *Curr. Opin. Chem. Biol.* **2014**, *23*, 1–7.

(71) Schüttelkopf, A. W.; van Aalten, D. M. F. PRODRG: a tool for high-throughput crystallography of protein-ligand complexes. *Acta Crystallogr., Sect. D: Biol. Crystallogr.* **2004**, *60*, 1355–1363.

(72) Schrödinger. *Maestro, Schrödinger Release 2017-2*; Schrödinger, LLC: New York, NY, United States, 2017.

(73) GraphPad. *Prism 7 for Mac OS X*; GraphPad Software: La Jolla, California, United States, 2017.

(74) Schrödinger. *The AxPyMOL Molecular Graphics Plugin for Microsoft PowerPoint*, version 1.8; Schrödinger, LLC: New York, NY, United States, 2015.